https://doi.org/10.5194/egusphere-2026-2313
Preprint. Discussion started: 27 April 2026
© Author(s) 2026. CC BY 4.0 License.

A composite-based analysis of the dynamical linkage of Atmospheric Rivers, Warm Conveyor Belts, and Extratropical Cyclones

Tiago M. Ferreira[1,2], Ricardo M. Trigo[1], Joaquim G. Pinto[2], Julian Quinting[2¤], Svenja Christ[2], and Alexandre M. Ramos[2]

[1]Instituto Dom Luiz, Faculdade de Ciências, Universidade de Lisboa, Lisbon, Portugal
[2]Institute of Meteorology and Climate Research – Troposphere Research (IMKTRO), Karlsruhe Institute of Technology (KIT), Karlsruhe, Germany
[¤]Current Address: Institute of Geophysics and Meteorology, University of Cologne, Cologne, Germany

Correspondence to: Tiago M. Ferreira (tiago.ferreira@partner.kit.edu)

Abstract. Extratropical cyclones (ETCs), warm conveyor belts (WCBs), and atmospheric rivers (ARs) are dynamically connected features key to understand midlatitude weather and hydroclimate. However, the precise spatial and temporal coupling between the moisture transport in ARs and the ascent in ETC's associated WCBs remains poorly understood. Therefore, this study employs a composite-based analysis, combining probabilistic footprints of WCB identification and Eulerian AR detection for the North Atlantic extended winter (October-March) using ERA5 reanalysis. We evaluate composite fields relative to AR centroids, differentiating between events where the WCB ascent phase is present within the AR plume from those where it is absent. Our results demonstrate that ARs linked to WCBs are characterized by stronger integrated vapor transport, a wider AR plume, and, most critically, a shift of precipitation maxima northeast of the AR axis, aligning with the region of strongest frontal ascent near the associated ETC. In contrast, AR-only events exhibit weaker IVT values and a diffuse precipitation to the northeast towards the cyclone. Finally, temporal composites centered on the ETC's maximum deepening point (MDP) reveal a phased evolution: while peak WCB-inflow precedes the MDP, peak WCB-ascent and AR-related precipitation coincide with the MDP, and peak WCB-outflow follows, illustrating a tightly coupled feedback loop.

1 Introduction

Extratropical Cyclones (ETCs) are responsible for significant weather hazards such as strong winds, extreme precipitation, and strong temperature gradients (Wernli et al., 2002; Fink et al., 2009; Pfahl et al., 2014). Climatologically, these cyclones develop preferentially along the Gulf Stream and North Atlantic Current, a region of enhanced baroclinicity, before tracking northeastward toward Iceland and the Norwegian Sea (Hoskins and Hodges, 2002; Ulbrich et al. 2009). This main storm track exhibits a distinct seasonal cycle, with maximum cyclone intensity and frequency during boreal winter due to a stronger meridional temperature gradient and an intensified jet stream (Ulbrich et al., 2009; Woollings et al., 2010). The variability of the North Atlantic storm track is closely linked to large-scale teleconnection patterns, such as the North Atlantic Oscillation (NAO), which modulates the latitudinal position and strength of cyclone activity (Trigo et al., 2002; Woollings and Blackburn, 2012). The classical structure of an extratropical cyclone is characterised by a warm front, a cold front, and a warm sector, features that were first synthesised in the Norwegian Cyclone Model nearly a century ago. As reviewed by Dacre (2020), subsequent observational and modelling studies have refined this conceptual view, revealing additional features such as the dry intrusion, the conveyor-belt airflow (warm and cold conveyors), and the occluded front. More recent research, summarised by Schultz et al. (2019), has emphasised that extratropical cyclones are fundamentally three-dimensional, tropopause-reaching structures. Their evolution is governed by the interaction between lower-tropospheric baroclinicity and upper-level potential vorticity anomalies.

Within these systems, two crucial moisture transport mechanisms are often present: warm conveyor belts (WCBs) and atmospheric rivers (ARs). Both WCBs and ARs play pivotal roles in the global hydrological cycle and are often associated with extreme weather events (Pfahl et al. 2014; Catto et al. 2015; Ramos et al. 2018a; Ramos et al. 2018b). Nevertheless, their

https://doi.org/10.5194/egusphere-2026-2313
Preprint. Discussion started: 27 April 2026
© Author(s) 2026. CC BY 4.0 License.

precise dynamical relationship remains an active area of research: although the definition of ARs (Ralph et al. 2018) states that they align with the low-level jet and warm sector of ETCs, the spatial coincidence between the core of maximum integrated vapor transport defining an AR and the region of strongest WCB ascent is often not given. Recently, it has been suggested that understanding the intricate interactions between ETCs, WCBs, and ARs is crucial for enhancing weather forecasting and climate projections (Lopez-Marti et al 2025).

Warm Conveyor Belts are coherent, rapidly ascending airstreams originating in the lower troposphere within the warm sector of an ETC, transporting warm, moist air poleward and upward towards the upper troposphere and lower stratosphere (Carlson 1980; Wernli 1997; Catto et al 2010; Wernli and Gray 2024). This ascent leads to significant latent heat release through condensation, which can intensify the cyclone and contribute to the formation of extensive cloud bands and precipitation (Binder et al 2016; Wernli and Gray 2024). The strength of WCBs has been moderately to strongly correlated with cyclone intensification, as quantified by the normalized maximum 24-hour central sea level pressure deepening (Binder et al 2016). Recent studies highlight that while classical WCBs are characterized by continuous ascent, embedded convection with ascent rates exceeding 50 hPa hr^{-1} can occur, influencing their moisture transport characteristics and cloud properties (Oertel et al 2019; Schwenk and Miltenberger 2024). Much of this embedded convection is organized by conditional symmetric instability (CSI), a slantwise instability common in midlatitude frontal zones that generates uplift and can locally intensify latent heat within the WCB ascent phase (Bennetts and Sharp 1982; Glinton et al. 2017). Moreover, the interaction between CSI and WCB ascent thus influences the vertical structure of moisture transport and may help explain spatial offsets between maximum ascent and maximum IVT (vertically integrated vapor transport). WCBs play a crucial role in redistributing moisture within cyclones, and kinematic analysis reveals how airflows within a cyclone's warm sector move rear-ward relative to the cyclone precipitation shield (Dacre et al 2019). The ascent timescales within WCBs are critical for understanding moisture transport into the upper troposphere and lower stratosphere, impacting cloud radiative forcing (Joos 2019; Schwenk and Miltenberger 2024).

Atmospheric Rivers are narrow, elongated corridors of concentrated water vapor transport in the troposphere, extending from subtropical to extratropical regions (Gimeno et al 2014; Dacre and Clark 2015; Ralph et al. 2018). These systems represent the high transport of moisture, accounting for the majority of poleward water vapor transport in the midlatitudes (Gimeno et al 2014; Dacre and Clark 2015). ARs are frequently associated with extreme precipitation events when they are forced upward, for example when they make landfall over mountainous terrain or by the influence of the WCB's ascent phase, leading to flooding and providing crucial water supply (Dacre and Clark 2015; Eiras-Barca et al 2016; Ralph et al 2018). They are usually identified using a threshold of IVT and are typically located in regions where their dynamical and thermodynamical components are relatively large throughout the depth of the lower troposphere (Dacre et al. 2019).

ARs can be considered as an integral part of the broader WCB system of ETCs (Dacre et al. 2015). Research indicates a strong statistical relationship between ARs and ETCs, with a pronounced cyclone typically located poleward and westward of the AR centroid and an anticyclone located equatorward and eastward of the AR (Guo et al 2020). This creates a strong horizontal pressure gradient that forces moisture to be transported within the warm sector of the cyclone, where the AR is present. While a significant majority (82%) of ARs are associated with an ETC, only about 45% of ETCs are paired with an AR, and the spatial relationship between them can vary considerably (Zhang et al 2019). Stronger ARs are frequently associated with explosive ETCs, with nearly 78% of ARs over the Northern Pacific being linked to strong ETCs (Eiras-Barca et al. 2018; Peng et al 2025). This suggests that more intense ARs are more closely related with more intense cyclones, contributing to extreme weather phenomena such as compound windstorm-flood events (Lopez-Marti et al 2025). ARs have also been analysed in comparison with extratropical fronts by Luis et al. (2025). They found that ARs are more frequently located closer to the cold front rather than the warm front. This region, closer to the cold front, is characterized by a higher precipitation occurrence. Despite these advances, critical knowledge gaps persist regarding the precise spatial and temporal coupling between ARs and WCBs. While it is well established that ARs are often collocated with the inflow region of WCBs

https://doi.org/10.5194/egusphere-2026-2313
Preprint. Discussion started: 27 April 2026
© Author(s) 2026. CC BY 4.0 License.

ahead of cold fronts (Dacre et al. 2019), the exact location of maximum ascent relative to the highest IVT remains ambiguous. Some evidence suggests that peak WCB ascent may occur along the flanks or leading edge of ARs rather than coinciding with the core of maximum moisture flux, potentially influenced by conditional symmetric instability or frontal forcing (Schwenk and Miltenberger 2024; Dacre and Clark 2025). Research has traditionally focused on either the dynamical structure of the cyclone and its WCB (Madonna et al., 2014; Oertel et al., 2020) or on the thermodynamical characteristics and hydrological impacts of the AR (Gershunov et al., 2017; Ralph et al., 2018; Ramos et al. 2018a, 2018b; Zavadoff and Kirtman 2020). To our best knowledge, a quantitative analysis that directly maps the Lagrangian analysis of the WCB onto the Eulerian AR detection has only been done by Sodemann et al. 2020, but only from an area/occurrence point of view. They found that, in winter, about 40% of ARs occur in isolation and that around 23% overlap with WCBs. Therefore, several research gaps persist: is the most vigorous WCB ascent co-located with the axis of maximum IVT that defines the AR core? Or does the ascent occur preferentially along the AR's flanks or leading edge, perhaps due to frontal dynamics or CSI?

In recent years, two different events, involving the connection between ARs, WCBs, and ETCs affected Portugal. Both resulted in new 24-hour precipitation records, the first in Lisbon, Portugal, in December 2022 (Ferreira et al. 2025a), and the second in the Madeira Island in June 2023 (Ferreira et al. 2025b). The authors provided evidence that for both events, the WCB's inflow and ascent phases were present within the AR itself, the convergence of air (WCB-inflow) created suitable conditions for moisture inflow, as the AR intensified on both moisture content and spatial extent, and also, the WCB-ascent phase might have helped to intensify the precipitation occurrence, leading to both extreme events. Based on the above, and to address the research gaps presented above, this study employs a composite analysis using reanalysis data to systematically quantify the relationship between the ascent (and inflow) phase of the WCB and the spatial structure of ARs. We move beyond a purely Eulerian analysis of IVT and precipitation fields by incorporating a Lagrangian-based identification of WCB trajectories (based on a probability footprint of the different phases of the WCB). By compositing fields of IVT, mean sea-level pressure, and precipitation relative to these identified ascent domains, we aim to elucidate the characteristic spatial pattern of ascent and its direct contribution to the total precipitation field.

We address the following research questions:

(1) How does the presence or absence of the WCB ascent phase influence the intensity and spatial distribution of precipitation within ARs, i.e., how different are the AR characteristics when the ascent phase is present within the AR?

(2) How does the AR-WCB association evolve during the lifecycle of the associated ETC particularly around the time of maximum deepening point (MDP)?

The structure of this manuscript is as follow: data and methods are presented in section 2; the climatological context and a case study are shown in section 3; the composite analysis from the AR perspective is detailed in section 4; the temporal evolution around the ETC's MDP is analysed in section 5; followed by conclusions in section 6.

2 Data and Methodology

2.1 Reanalysis Data – ERA5

The data used in this study to describe the large-scale flow is the ECMWF (European Centre for Medium-Range Weather Forecasts) Reanalysis v5 (ERA5; Hersbach et al., 2020). Several fields are extracted from both the surface and at specific atmospheric levels. The former includes the mean sea level pressure (SLP) and total precipitation. The latter include the zonal and meridional components of the vertically integrated water vapor transport (IVT, considering the entire atmospheric column). All these fields are obtained with a 0.25º latitude-longitude grid spacing and a 6-hourly temporal resolution. The IVT corresponds to the following metrics:

https://doi.org/10.5194/egusphere-2026-2313
Preprint. Discussion started: 27 April 2026
© Author(s) 2026. CC BY 4.0 License.

$$IVT = \sqrt{{u_q}^2 + {v_q}^2}\,, \tag{1}$$

with

$$u_q = IVT_u = \frac{1}{g}\int_{ps}^{p} uqdp\,, \tag{2}$$

and

$$v_q = IVT_v = \frac{1}{g}\int_{ps}^{p} vqdp\,, \tag{3}$$

where g is the gravitational acceleration, q is the specific humidity, ps is the surface pressure, p is maximum pressure (usually 300 hPa), and u and v are the zonal and meridional wind components (Lavers et al., 2012). This field is internally computed by the ECMWF, from the surface to the top of the atmosphere (1hPa), considering all 37 pressure levels available in ERA5. While the upper layer of the atmosphere holds very little humidity, using the full column is standard practise and computationally efficient, as ERA5 provides IVT_u and IVT_v as pre-computed, vertically integrated fields: 'vertical integral of eastward water vapor flux' (IVT_u) and 'vertical integral of northward water vapor flux' (IVT_v).

The analysis is applied to the entire North Atlantic basin and the western and central regions of Europe, ranging from 100ºW to 40ºE and 0 to 90 ºN, considering only the extended winter season (from October to March).

2.2 AR Detection method – IPART

For the detection of AR events, we have implemented and adapted the global AR tracking method developed by Xu et al. (2020) and widely used in recent years (e.g., Fernández-Alvarez et al. 2023; Ferreira et al. 2025a, 2025b). The detection algorithm is based on thresholds at the spatiotemporal scale of ARs and is independent of the IVT thresholds. IPART (image-processing-based atmospheric river tracking method) is inspired by the 'Top Hat by Reconstruction' technique (Vincent, 1993), which involves subtracting a greyscale reconstruction by dilation image from the original image. This greyscale reconstruction by dilation image is the background IVT content and the original image is the non-negative IVT distribution. The difference between these two components is the transient IVT component, which includes AR candidates. The output of this step is a decomposition of IVT into a reconstruction component and the anomaly component, in which the ARs are searched for. A threshold of 200 kg m^{-1} s^{-1} is applied to the anomaly field, and for each region the standard criteria for AR detection (length ≥ 2000 km; width < 1000 km; length/width ratio > 2) are implemented. More details on this method can be found in Xu et al. (2020). Additionally, in order to exclude tropical cyclones from the analysis, we apply both a circularity criterion with a maximum value of 0.5 (following the work of Mahto et al. 2023) and a minimum value of 1000 km to the distance between the first and last points of the AR axis, ensuring that the feature is a long, filamentary plume, distinct from the closed circulation typical of tropical cyclones. Here, an AR object corresponds to an AR detected at a timestep and an AR event as the entire lifecycle tracking. A key advantage of IPART is that unlike conventional methods, it is less dependent on magnitude thresholds, detecting ARs based on their spatial 'spikiness' rather than absolute moisture values. This makes it more robust for detecting ARs in both midlatitude and polar systems, without changing settings, and in a warming climate where atmospheric moisture levels are expected to increase (Lu et al. 2025). The filtering process is relatively insensitive to the size/shape of the structuring element, providing greater tolerance to varying water vapor flux intensities. Also, the new axis identification method provides a physically correspondent axis that follows major flow directions, stays close to the maximum flux values, handles complex shapes, and never extends out of the AR boundary.

https://doi.org/10.5194/egusphere-2026-2313
Preprint. Discussion started: 27 April 2026
© Author(s) 2026. CC BY 4.0 License.

2.3 WCB Identification - ELIAS

The method ELIAS (EuLerian Identification of Ascending AirStreams), developed by Quinting and Grams (2022), uses convolutional neural networks to predict the conditional probabilities of the WCB inflow, ascent, and outflow footprints. The model was trained on a labelled dataset where the 'ground truth' for each WCB stage was defined using Lagrangian trajectories, computed with the LAGRANTO algorithm (LAGRangian ANalysis TOol; Wernli and Davies, 1997; Sprenger and Wernli, 2015) on a 1º x 1º horizontal grid. These trajectories were derived from Madonna et al. (2014) and extended to 2016 by Sprenger et al. (2017). A trajectory was classified as a WCB if it ascended by at least 600 hPa in 48 hours and was matched with an extratropical cyclone. Based on this, the WCB inflow is defined as the part of the WCB in the lower-troposphere (below 800 hPa), originating from the boundary layer in the warm sector of ETCs (it is the convergence of warm, moist air into the ETC), the WCB ascent as the part of the WCB between 800 and 400 hPa, ascending across the cyclone's warm front, and the WCB outflow for above 400 hPa, reaching the upper troposphere. ELIAS, which uses these trajectory-derived labels, employs five predictors for its deep learning model: (1) four are derived from temperature, geopotential height, specific humidity, and the horizontal wind components at 1000, 925, 850, 700, 500, 300, and 200 hPa isobaric surfaces and (2) the fifth is a 30-day running mean trajectory-based climatological of WCB occurrence frequency. This set of inputs allows ELIAS to provide a computationally efficient and consistent Eulerian alternative to traditional Lagrangian trajectory calculations, offering a probabilistic footprint of WCB stages that is highly suitable for large-scale composite analysis. The approach has been applied to ERA5 and compared with the original data by Christ et al. (2025), who found the results to be consistent.

2.4 ETC tracking method

The ETC tracks used in this study are based on the algorithm described by Pinto et al. (2005) based on Murray and Simmonds (1991). The algorithm is applied to the Northern Hemisphere (20 to 90 ºN) and involves a multi-step approach, primarily focusing on the Laplacian of mean sea level pressure (∇^2SLP). The process begins with the identification of local maxima in the ∇^2SLP field across the Northern Hemisphere. These maxima indicate regions of intense cyclonic circulation. Subsequently, the algorithm searches for corresponding minima in the raw SLP field that are in close vicinity to these ∇^2SLP maxima. This step is crucial because while ∇^2SLP efficiently pinpoints the strongest cyclonic gradient, the actual center of a low-pressure system, which defines a cyclone's core, is an SLP minimum. The relationship between ∇^2SLP and SLP minima is key for associating the mathematical detection with a 'real' low-pressure core, indicative of a closed-system cyclone. If an SLP minimum is found within a specified vicinity of a ∇^2SLP maximum, they are combined to represent a single cyclone track. To ensure that only synoptically significant cyclones are analysed, several filtering criteria are applied to the identified tracks. A minimum lifetime of 24 hours is imposed, eliminating short-lived systems that typically do not contribute significantly to large-scale weather patterns. Furthermore, a minimum intensity threshold is applied, requiting the lifetime maximum ∇^2SLP to be greater than or equal to 0.6 hPa/(degree latitude)^2, filtering out weak systems. A minimum deepening rate is also considered, specifically a maximum $\frac{d}{dt}\nabla^2 SLP \geq 0.3$ hPa / (degree.latitude)^2 over a 24-hour period (Pinto et al. 2009). This criterion captures rapidly intensifying cyclones, often referred to as 'explosive cyclones'. An additional filter requires a minimum travel distance of at least 1000 km. This ensures that only systems with a sustained trajectory are considered, excluding stationary lows. Topographic influences are also accounted for by discarding cyclones located over high orography, specifically above 1500 meters. Only the cyclones that are considered as closed systems are used on this study. For this, the algorithm searches the spline interpolated field for a pressure minimum in the vicinity of the ∇^2SLP maximum in order to associate the latter with a 'real' low pressure core. If such a minimum is found, the cyclone is classified as a closed system, with its core located at the pressure minimum. Finally, any cyclones whose strength, measure by ∇^2SLP, does not reach

https://doi.org/10.5194/egusphere-2026-2313
Preprint. Discussion started: 27 April 2026
© Author(s) 2026. CC BY 4.0 License.

0.1 hPa / (degree.latitude)^2 are also eliminated. This cyclone tracking approach compares well with other methods, particularly for strong long living systems during the central part of their lifetime (Neu et al., 2013).

2.5 Assignment of ARs to ETCs

In order to associate each AR object to an ETC, for every AR object several conditions are assessed:

(1) If there is only 1 ETC at a maximum distance of 2000 km from the AR centroid, the association is straightforward.
(2) If there is more than 1 ETC, the AR is associated to the one that has the lowest SLP.
(3) If there is no ETC within a 2000 km radius of the AR, then the maximum distance is increased to 4000 km, and the search process is redone. If there is still no ETC, the AR is saved as not associated.
(4) Then, if an AR event is associated to more than 1 ETC throughout its lifecycle, the AR is associated to the one that had the most concurrent timesteps. This helps avoiding duplicated data on the composite analysis.

This procedure successfully associated approximately 99.2% of all ARs events with an ETC. Finally, all cyclone tracks are evaluated relative to the time of their peak intensity, which is defined as MDP (Maximum Deepening Point) throughout this study. Timesteps before (after) peak intensity are indicated as MDP -xxh (MDP +xxh) to peak intensity.

2.6 Rotation Methodology

Following the identification of AR objects, we standardized their geometric orientation for robust composite analysis. This procedure was adopted to mitigate the confounding effects of varying AR axis directions on the composite structure, ensuring that the resulting patterns reflect intrinsic physical relationships rather than geometric aliasing.

In Dacre et al. (2019), cyclone composites were calculated by considering the direction of movement on the time of maximum intensity of each cyclone. As such, the direction applied to the rotation becomes the same for all cyclones. Contrary to them, and following the work of Asharaf et al. (2024), the rotation was performed individually for each AR object at its respective timestep, for the associated environmental fields (including IVT, SLP, and precipitation) and also for the WCB at the same time step. The core of this transformation involves a two-stage process:

1. Each AR object was rotated by an angle of (90º - θ), where θ is the object's primary directional orientation. This calculation effectively reorients all AR objects to a common west-to-east orientation within the composite framework, aligning their moisture plumes along a standardized longitudinal axis. (This transformation is illustrated on Figure 1. For a given timestep, the original fields (Figure 1a) are rotated such that the AR's primary axis is aligned zonally (west-to-east) within the composite framework (Figure 1b)); and
2. To account for the convergence of meridians in the spherical coordinate system and the resulting reduction in zonal grid spacing with increasing latitude, all rotated fields were normalized by the cosine of the latitude (cos(φ)). This essential adjustment rectifies the areal distortion inherent in latitude-longitude grids, ensuring that quantitative measures of flux and intensity are conserved and comparable across the composite domain.

The final output of this preprocessing step is a set of standardized, rotated fields for each AR event, all centered on the AR's centroid and aligned along a uniform directional axis. This object-based, rotated framework provides a consistent coordinate system, which is a prerequisite for a meaningful composite analysis. It allows for the precise examination of the spatial co-location between the axis of maximum IVT and the regions of most vigorous WCB ascent, free from the directional variability of individual events.

https://doi.org/10.5194/egusphere-2026-2313
Preprint. Discussion started: 27 April 2026
© Author(s) 2026. CC BY 4.0 License.

2.7 Composite Methodology

The core of our diagnostic approach involves the construction of Eulerian composite to elucidate the three-dimensional structure of the coupled AR-WCB system. This technique allows us to statistically synthesize the key atmospheric fields around a common reference point, revealing the characteristic spatial patterns that define the interaction. The composite analysis was performed separately for two distinct populations to enable a comparative assessment:

1. **Definition of event classes:** at each 6-hourly analysis timestep, all identified AR objects were classified into one of two categories based on the presence of the WCB's ascent phase:
    a. Coupled AR-WCB events: AR objects that are co-located with a diagnosed WCB ascent region (inside the green box in Figure 1a and 1b, i.e., an overlap of any WCB ascent grid point with the AR object).
    b. AR-only events: AR objects where the WCB ascent phase is absent or far from the AR.
2. **Grid extraction and alignment:** for each event in both classes, a regional domain of fixed size was extracted from the global fields. The centroid of the AR object was used as the central point, placed at the geometric origin (0,0) of a standardized composite grid. This alignment ensures that the composite mean reflects the typical spatial organization of variables relative to the AR's centroid.
3. **Composite mean calculation:** the final composite fields for each event class were generated by computing the arithmetic mean of all aligned grids. This process yields a statistically representative model of the atmospheric state for each class, effectively filtering out the noise of individual case-specific features and highlighting the robust, systematic signals of the AR-WCB interaction.

This stratified compositing approach is designed to isolate the unique fingerprint of the WCB's dynamical forcing on AR structure. By comparing the composite fields of coupled AR-WCB events against those of AR-only events, we can quantitatively attribute differences in the patterns of vertical motion, precipitation, and integrated vapor transport directly to the influence of the ascending airstream.

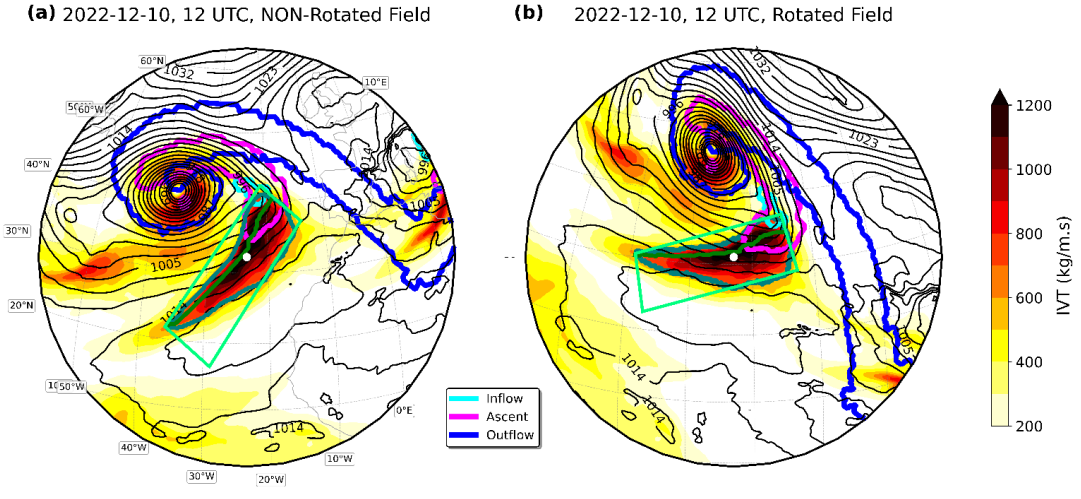

Figure 1: Schematic of the rotational composite methodology. (a) Original fields for a case study on 10 December 2022, 12 UTC, showing an atmospheric river (AR, dark-green contour), the warm conveyor belt (WCB) inflow (light blue), ascent (pink), and outflow (blue) phases, sea-level pressure (SLP, black contours), and IVT (shaded in kg m^{-1} s^{-1}). The ETC center is located northwest of the AR. The light-green box denotes the search region for WCB ascent influence. The white point marks the AR centroid and the green line inside the AR represents its axis. (b) The same fields after application of the rotational and latitude-correction algorithm, aligning the AR axis zonally (west-to-east, green line inside the AR) for compositing.

https://doi.org/10.5194/egusphere-2026-2313
Preprint. Discussion started: 27 April 2026
© Author(s) 2026. CC BY 4.0 License.

3 Climatological context and case study analysis of AR-WCB-ETC interactions

3.1 Climatological Overview

The extended winter climatology of ARs, WCB phases, and ETCs are displayed in Figure 2, revealing a coherent, co-located spatial pattern across the North Atlantic. All features exhibit maximum frequency along a southwest-northeast corridor extending from the Gulf Stream region towards Iceland and northwestern Europe. The peak of WCB inflow occurrence (Figure 2b) at ~37°N, 73°W aligns precisely with the Gulf Stream's western extension, a well-known region for cyclogenesis (Schemm and Sprenger 2015; Coll-Hidalgo et al. 2024; Ma et al. 2024). Eastward of the inflow highest climatology, the AR, WCB-ascent, and ETC climatologies peak (Figure 2c, 2d, 2a, at ~40°N, 45°W, ~45ºN,43°W, and 50ºN,45°W, respectively), exhibiting a ~10º latitudinal offset that is dynamically consistent with the structure of a mature ETC. The AR is positioned within the cyclone's warm sector, typically to the south and southwest of the low-pressure centre (Eiras-Barca et al. 2018; Zhang et al. 2019) This location places it directly within the path of the WCB's low-level inflow. The WCB-ascent, in turn, occurs just ahead of the surface cold front, embedded within the high IVT corridor of the AR. ERA5-based WCB climatologies confirm that this ascent is collocated with zones of strongest IVT convergence, where large-scale uplift is most pronounced (Heitmann et al 2024). The ETC peak occurs further poleward, completing the spatial alignment between the 3 systems. This entire co-occurrence is often situated beneath the upper-level Atlantic jet stream, specifically the left-exit or right entrance regions, where upper-level divergence forces low-level convergence and ascent, thereby deepening the surface low (Uccellini and Johnson 1979; Winters 2021).

The variability of the outflow climatology (Figure 2f) stems from both methodological limitations and physical complexity. ELIAS 2.0, while state-of-the-art in identifying WCB footprints via deep learning, does not resolve the bifurcation into cyclonic versus anticyclonic branches, an essential distinction because the anticyclonic outflow contributes disproportionately to upper-tropospheric ridge building and blocking anticyclone formation (Heitmann et al. 2024; Vishnipriya et al. 2025). The observed outflow maximum southeast of Greenland likely represents the anticyclonic branch, where WCB air, having crossed the tropopause, exports mass and momentum into the subtropical jet stream, influencing downstream Rossby wave evolution (Saffin et al. 2021). This explains why outflow appears more diffuse: it is sensitive to tropopause folding, jet stream position, and stratosphere–troposphere exchange, processes less constrained by surface forcing than inflow or ascent.

Both AR (Figure 2c) and ETC (Figure 2a) climatologies follow the same spatial pattern. While only about 30.5% of all ETCs have an associated AR, a remarkable 99.2% of detected ARs are linked to an ETC. This underscores that almost every AR in this region is an integral component of a larger synoptic-scale cyclonic system, acting as its primary moisture reservoir. The subset of ETCs that have an associated AR preferentially forms in the western North Atlantic (Figure 2e), directly over the Gulf Stream, where high SSTs (not shown) provide the necessary moisture to develop an AR (Lopez-Marti et al., 2026).

3.2 Illustrative Case Study: February 2010

In Figure 3, a case study from 2-6 February 2010 illustrates the typical development/lifecycle of an WCB/ETC/AR coupled system. On 2 February, 06UTC (Figure 3a), a large-scale inflow region can be observed at low latitudes off the east coast of North America. On 3 February, 00UTC (Figure 3b), the vertically coherent organization of the WCB, where parcels rapidly transition from boundary layer inflow to significant ascent and ultimately upper-tropospheric outflow, can be observed just off the east coast of North America, depicting the cyclogenesis of an ETC. One day after, on 4 February, 00UTC (Figure 3c), the cyclone centre emerges at 60ºW,38ºN (with a minimum value of 980 hPa) with a region of high integrated water vapor transport to its southeast with values above 700 kg m^{-1} s^{-1}. This high moisture transport combined with the large convergence in the WCB inflow region allows the detection of an AR on 5 February, 00UTC. On that day (Figure 3d), we can clearly see the collocation between the ETC, WCB and AR: (1) diabatic heating in the WCB ascent close to the cyclone centre probably intensifies the cyclone development (to 949 hPa); (2) the WCB ascent is located in the AR region which is at the typical

https://doi.org/10.5194/egusphere-2026-2313
Preprint. Discussion started: 27 April 2026
© Author(s) 2026. CC BY 4.0 License.

southwestern side of the cyclone; and (3) the inflow phase coinciding with most of the AR area, allowing it to develop and intensify. The ascent and inflow move eastward with the AR; the AR intensifies on both moisture content and spatial extent (on 6 February, 00UTC, Figure 3e) and moves further east from the ETC. On 7 February, 00UTC (Figure 3f), the AR is no longer influenced by both the inflow nor the ascent and begins to lose moisture as it moves closer to the European continent.

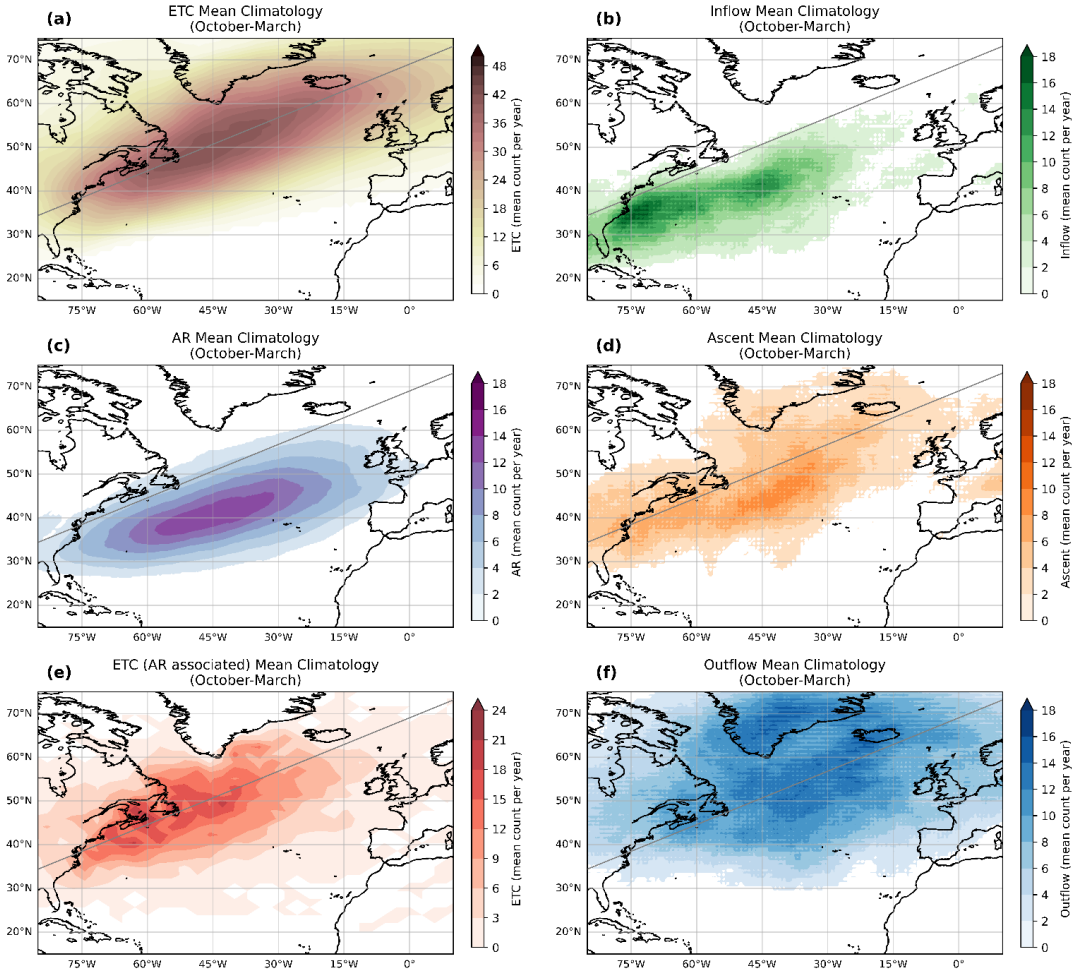

Figure 2: Extended winter (October-March) climatology (1979-2023) of (a) all Extratropical Cyclones (ETC) frequency, (b) WCB inflow frequency, (c) Atmospheric River (AR) frequency, (d) WCB ascent frequency, (e) frequency of ETCs associated with an AR, and (f) WCB outflow frequency. Note the coherent spatial pattern from the Gulf Stream region northeastward, with AR and WCB inflow maxima positioned downstream of the primary SST gradient and upstream of the peak ETC and WCB ascent activity. Grey line represents the axis of the ETC climatology's distribution showed in (a), for easier orientation.

https://doi.org/10.5194/egusphere-2026-2313
Preprint. Discussion started: 27 April 2026
© Author(s) 2026. CC BY 4.0 License.

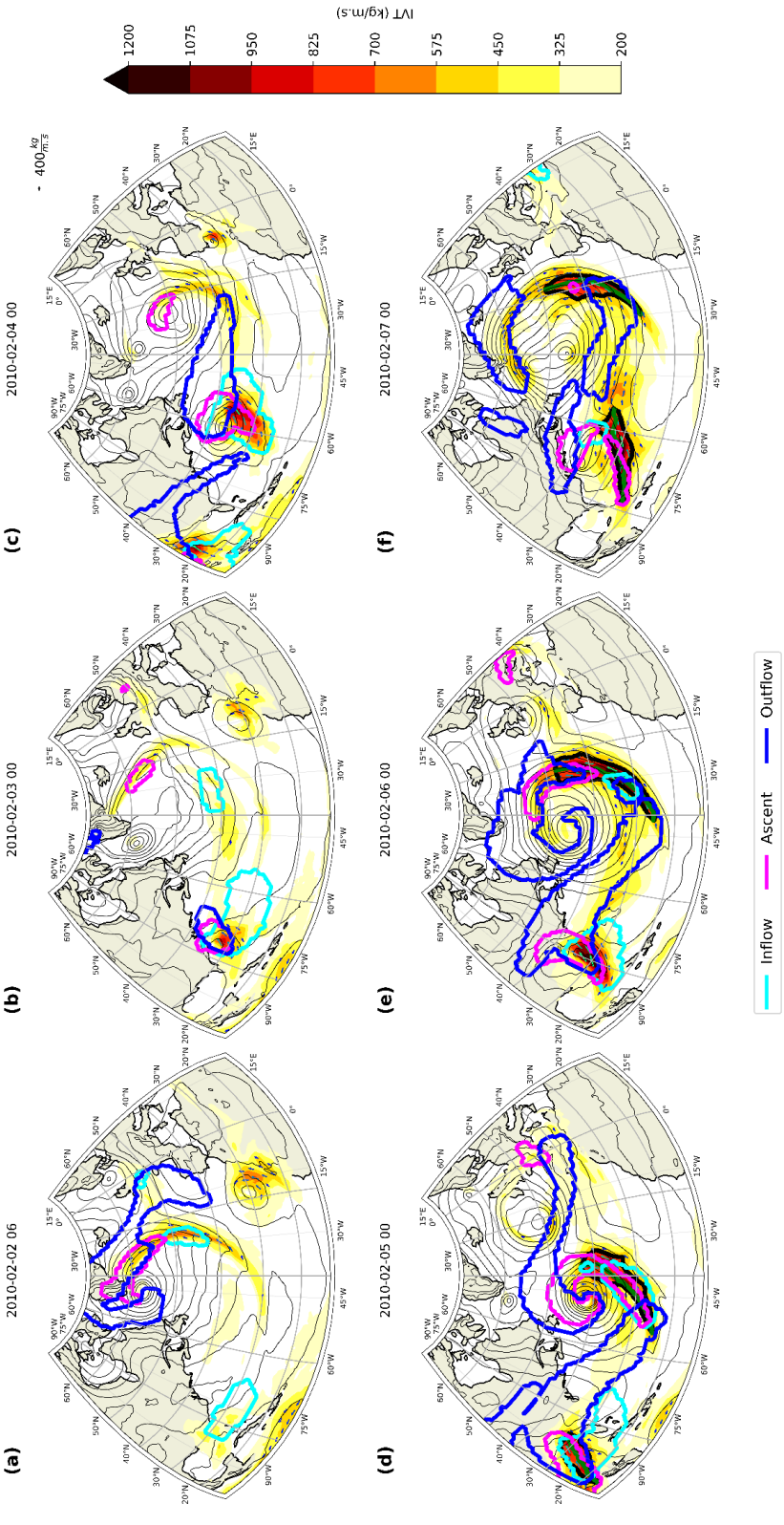

Figure 3: Case study of a coupled AR-WCB-ETC event in February 2010. Panels show the evolution from 2 February (06 UTC) to 6 February (00 UTC). Black contours show sea-level pressure (SLP), with the bold contour indicating the detected AR boundary. WCB phases are shown as inflow (light blue), ascent (pink), and outflow (blue). Shading shows IVT. The sequence illustrates cyclogenesis (3 Feb), the emergence of a strong AR coincident with cyclone intensification (4-5 Feb), and the subsequent decay phase where the AR detaches and makes landfall.

https://doi.org/10.5194/egusphere-2026-2313
Preprint. Discussion started: 27 April 2026
© Author(s) 2026. CC BY 4.0 License.

4 The role of WCB ascent: Composite analysis from the AR perspective

In this section we compute several rotated composites (from the viewpoint of the AR) of relevant variables for the study of ARs, differentiating between ARs that are influenced by the ascent phase of the WCB and ARs where the WCB's ascent phase is absent (see section 2.7). Critically, the distinction between WCB-influenced and WCB-absent ARs is not merely semantic: it reflects fundamentally different thermodynamic and kinematic regimes governing moisture conversion efficiency, storm-scale feedback, and downstream flow evolution (Heitmann et al. 2024; Federer et al. 2025). To note that values presented throughout the rotated composites correspond to mean values on each AR object.

4.1 Composite Structure of key fields

The rotated SLP composite (Figure 4a and 4b), confirm the synoptic pattern for both AR types: a cyclone situated poleward and westward of the AR centroid and an anticyclone to the south and east. According to Guo et al. (2020), this dipole (cyclone located poleward and westward of the AR centroid and anticyclone equatorward and eastward) leads to strong horizontal pressure gradient that forces moisture to be transported along a narrow corridor within the warm sector of the cyclone (with a W-E direction in this rotated framework). However, the differences in the cyclone's proximity and intensity between the two composites suggest that WCB-influenced ARs occur closer to cyclones, which provides the stronger dynamical forcing necessary to sustain the intense WCB ascent.

The IVT rotated composites (Figure 4c and 4d) highlight a quantitative difference in moisture intensity. In WCB-influenced cases, the core IVT exceeds 1100 kg m^{-1} s^{-1}, a threshold significantly higher than the sub-1100 kg m^{-1} s^{-1} values observed in WCB-absent cases. This enhancement is not just a matter of intensity, as the spatial structure is also altered. The relative frequency contours of the AR itself are broader in the influenced cases, suggesting a larger spatial footprint. This expansion is likely a direct consequence of the intensified low-level convergence associated with the WCB-inflow phase (Figure 5a), that draws in and concentrates water vapor over a wider area. The data shows that the inflow phase occurs over 40% of the time north of the AR core in influenced cases, compared to a mere 10% in absent cases, providing a clear kinematic explanation for the observed differences in AR width and intensity.

The most profound and operationally significant finding emerges from the precipitation composites (Figure 4e and 4f). In WCB-influenced ARs, precipitation maxima exceeding 8 mm are not centred on the AR's IVT maxima (the origin point (0,0)) but are instead displaced to the northeast, forming a distinct plume that extends toward the surface cyclone centre (located at approximately (350, 1050) km in the rotate frame Figure 4e). This spatial offset is a direct manifestation of the synoptic-scale dynamics: the heaviest precipitation occurs where the poleward-advected moist air within the AR encounters the strongest large-scale ascent, typically along and just ahead of the cold front of the associated ETC. In contrast, WCB-absent ARs (Figure 4f) produce a much weaker and more diffuse precipitation signal, with values generally below 5 mm within the AR and extending northward, with only 2-3 mm, connecting to the cyclone. This weak signal likely arises from less efficient mechanism like broad slantwise ascent or residual frontal lift, which lack the focused, enhanced vertical motion characteristics of a WCB.

From these composites we can observe that while there are large amounts of water vapor on both AR cases, the presence of the ascent phase plays an important role for the occurrence of large precipitation values. Its higher presence on the AR-influenced cases is probably due to the occurrence of the ETC closer to the AR (Figure 4a and 4b).

https://doi.org/10.5194/egusphere-2026-2313
Preprint. Discussion started: 27 April 2026
© Author(s) 2026. CC BY 4.0 License.

4.2 Spatial Co-location of WCB Phases

For the three phases of the WCB rotated composite (from the AR point of view), we combined the WCB masks based on the spatial alignment between the two systems, i.e., the values shown on Figure 5 represent the relative frequency of the WCB per AR object.

Starting with the inflow phase, for the WCB-influenced cases (Figure 5a), we can observe that convergence occurs above 40% to the northward side of the AR core, between the 70 and 90% of the AR relative frequency isolines, and spreads westward following a similar spatial extension as the AR relative frequency. As per the WCB-absent cases (Figure 5b), the inflow is substantially reduced occurring at a maximum of 10%. It should be noted that WCB-influenced cases correspond to 16852 AR objects and the WCB-absent to 3883 AR objects (an AR object correspond to one time step case detection). For the ascent phase, the WCB-influenced composite (Figure 5c) shows a clear resemblance with the precipitation composite (Figure 4e), with the highest occurrences within the AR contour but extending northward towards the cyclone. On Figure 5d, the WCB-absent ARs are generally located close to the lowest SLP values of Figure 4d with a percentage of 5-10% of occurrence. For the outflow phase, the WCB-influenced composite (Figure 5e) shows a 15% higher occurrence at the leading edge of the AR, than the WCB-absent cases. On the contrary, the WCB-absent cases seem to occur further from the AR. The large difference on the number of AR objects (16852 WCB-influenced, and 3883 WCB-absent) underscores that the vast majority of impactful ARs are dynamically coupled to a WCB. This demonstrates that while an AR provides the essential moisture reservoir, it is the WCB's ascent phase that converts moisture into precipitation. To note that this result is valid in the absence of orography. Contrary to the western coast of North America, where topography acts as an uplift mechanism for extreme precipitation to occur, on western Europe the dynamical mechanism (the ascent phase) might be more important for the occurrence of EPEs.

The composite results demonstrate that the WCB ascent is not merely spatially co-located and correlated with but clearly suggests, from its location, that it plays a critical role for transforming an AR moisture into a possible extreme precipitation event. The displacement of the heaviest precipitation northeast of the AR's IVT axis underscores that the core of maximum moisture flux and the region of most vigorous ascent are frequently misaligned. This has direct forecasting implications: assuming precipitation is co-located with the IVT maximum would lead to significant forecast errors. The weak precipitation in AR-only events likely results from synoptic-scale slantwise ascent or residual frontal lift, which is less efficient at converting moisture to rainfall than the focused, convective-enhanced ascent within a WCB (Oertel et al. 2021).

https://doi.org/10.5194/egusphere-2026-2313
Preprint. Discussion started: 27 April 2026
© Author(s) 2026. CC BY 4.0 License.

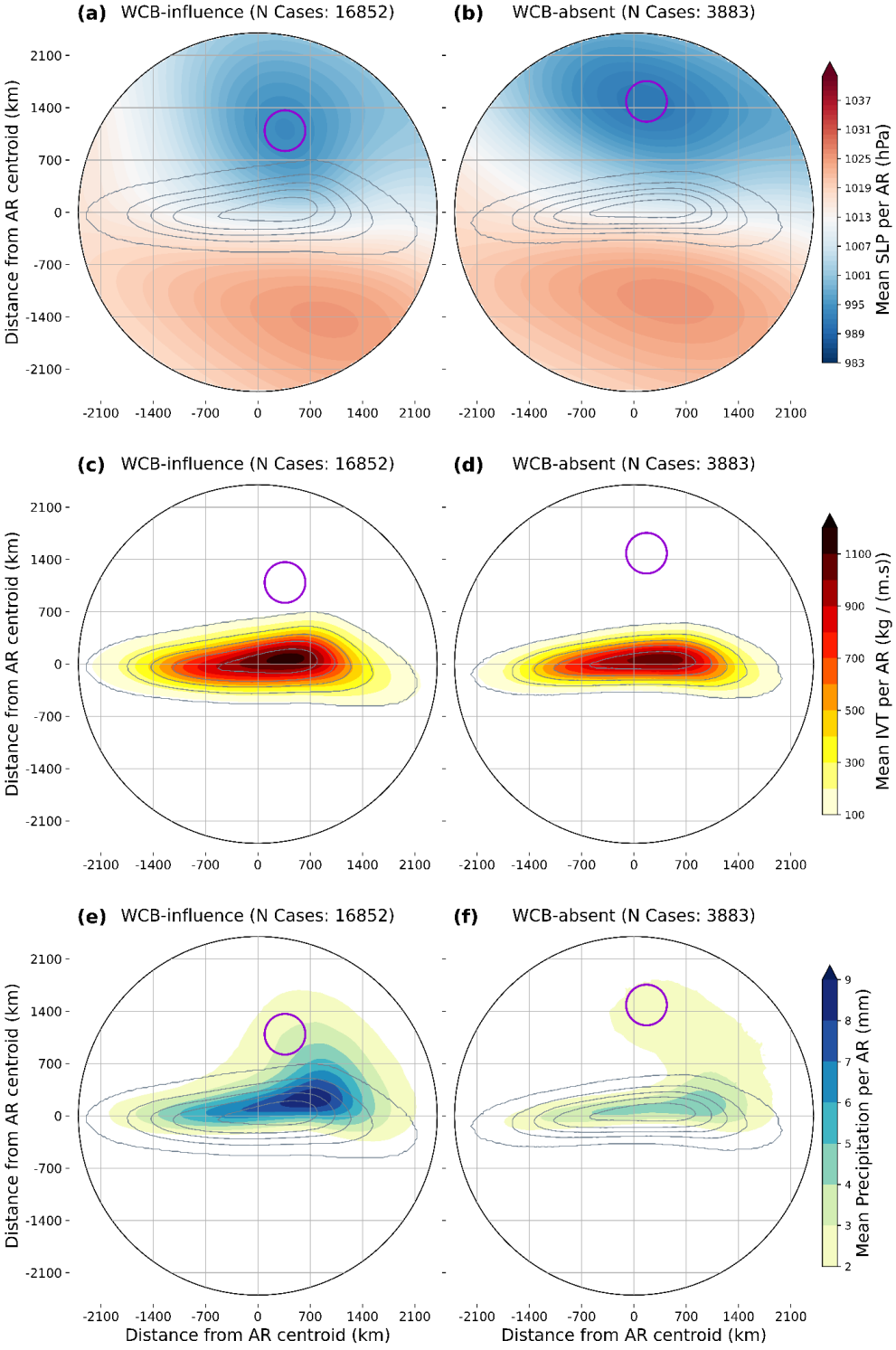

390 Figure 4: Composite fields centered on AR centroids for events with (left column) and without (right column) the WCB ascent phase. (a, b) Sea-level pressure (hPa). (c, d) Vertically integrated water vapor transport (IVT, kg m^{-1} s^{-1}).(e, f) Total precipitation (mm). Grey contours show the relative frequency of AR occurrence (10% to 90% intervals). The (0,0) point marks the AR centroid.

https://doi.org/10.5194/egusphere-2026-2313
Preprint. Discussion started: 27 April 2026
© Author(s) 2026. CC BY 4.0 License.

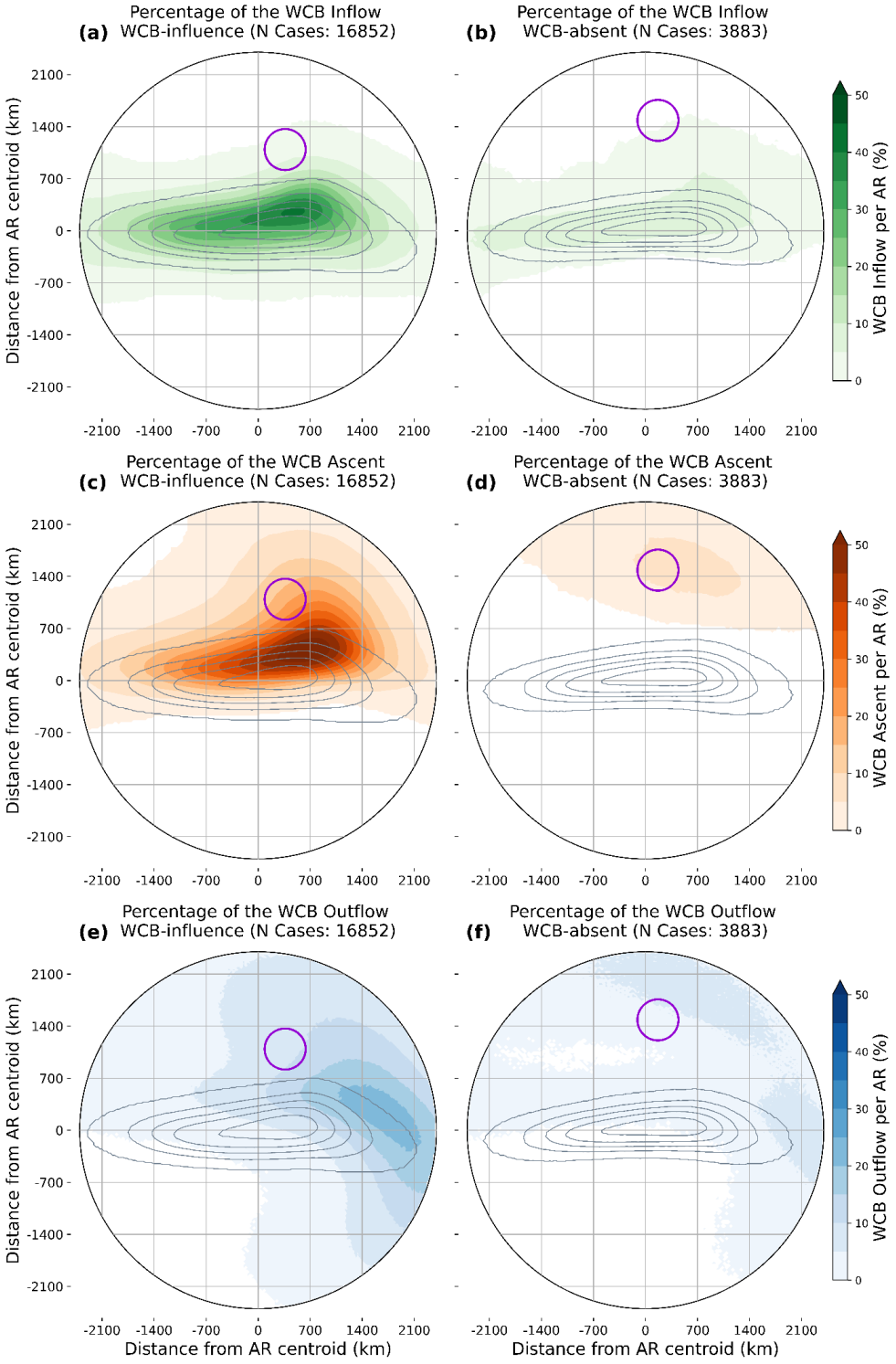

Figure 5: Composite frequency of occurrence (%) for each WCB phase, aligned with the AR-centered composites in Fig. 4. (a, b) WCB inflow. (c, d) WCB ascent. (e, f) WCB outflow. Left column: AR events with WCB ascent influence. Right column: AR-only events.

https://doi.org/10.5194/egusphere-2026-2313
Preprint. Discussion started: 27 April 2026
© Author(s) 2026. CC BY 4.0 License.

5 How does the AR characteristics varies throughout the ETC intensification?

Based on the previous results, we now take a closer look at the variation of the 12-hourly composites at (and around) the MDP of each ETC that has an associated AR, from -24h to +24h from the MDP, each 12h to better understand how the AR-WCB coupling evolves dynamically with time. Only the AR cases that are influenced by the ascent phase are analysed in this section.

5.1 Evolution of the WCB

The WCB inflow frequency peaks before the MDP (at MDP−24 h and MDP−12 h, Figure 6a, 6b). During this period, moist air is drawn into the developing warm sector, leading to an increase in column-integrated water vapor and, consequently, the formation and development of the AR. The WCB ascent frequency reaches its peak at the MDP and +12 h (Figure 6h, 6i) coinciding precisely with the IVT and precipitation maxima. This confirms the critical role of the WCB ascent in generating high precipitation and latent heat release, which in turn amplifies cyclone deepening, highlighting its role on generating high precipitation. Finally, the WCB outflow frequency increases and shifts downstream from the MDP onwards (Figure 6m, 6n, 6o).

This phased evolution outlines a feedback loop: intense moisture convergence (inflow) feeds both the AR and the cyclone. Diabatic release in the WCB ascent intensifies the cyclone (peaking at MDP) and generates intense precipitation within the AR. Finally, the cyclone's modification of the upper-level flow (outflow) begins to alter the large-scale environment, contributing to the system's decay. This tight temporal coupling, occurring within ±12-hour windows, underscores that the AR, WCB, and ETC should be considered an integrated, co-evolving system rather than independent features. The dynamic interactions between these components are critical, as errors in forecasting the jet stream that steers an AR, or inaccuracies in estimating moisture availability, can lead to significant forecast errors. Understanding these coupled dynamics is essential for improving predictions of extreme weather events associated with atmospheric rivers.

5.2 Evolution of IVT and Precipitation

Throughout the intensification of an extratropical cyclone, the associated AR exhibits a coherent structure, with IVT values consistently around 1000 kg m^{-1} s^{-1} over a 48-hour period centred on the cyclone's MDP (Figure 7a-7e). This persistence of high IVT, peaking precisely at the MDP, suggests that the AR reaches a near-saturated intensity state when the cyclone undergoes its most rapid intensification. The spatial extent of these ARs remains relatively consistent, spreading approximately 4200 km zonally (from -2100 km to +2100 km) and 1400 km meridionally (between -700 km and +700 km). The IVT is a crucial metric for ARs, quantifying the horizontal flux of water vapor through the atmospheric column, which is distinct from precipitable water, the total moisture content. The magnitude of IVT is expected to increase with temperature due to the Clausius-Clapeyron relation, implying that warmer conditions would lead to more intense ARs. Note that the number of cases varies considerably from -24h to +24h of the MDP: the maximum occurs on the MDP, with 1343 cases, and the minimum at MDP +24h, with 266 cases.

The evolution of precipitation within the AR-ETC system (Figure 7f-7j) provides a more detailed view of this coupling. At 24 hours prior to the MDP (Figure 7f), precipitation is relatively modest, approximately 6 mm/AR, and spatially confined near the AR axis. As the cyclone intensifies towards the MDP, precipitation significantly increases to over 7 mm/AR and expands spatially, mirroring the characteristic shape of the WCB ascent region (Figure 6h). This transition indicates a shift from frontal precipitation to precipitation generated within the WCB ascent. The precipitation maximum remains strong at MDP+12h before gradually decaying, aligning with the declining WCB ascent frequency and increasing outflow dominance. Latent heat release through condensation in the WCB ascent enhances cyclone deepening, creating a positive feedback loop where strong ascent leads to more latent heat, which deepens the low, which in turn strengthens the pressure gradient and the low-level

https://doi.org/10.5194/egusphere-2026-2313
Preprint. Discussion started: 27 April 2026
© Author(s) 2026. CC BY 4.0 License.

inflow, feeding even more moisture into the system. This explains why the most extreme precipitation events are linked to the MDP of the associated ETC (McErlich et al. 2023).

5.3 Precipitation and MDP distribution around AR's peak intensity

Synthesizing the findings presented above and in section 4, Figures 8 and 9 illustrate the relationship between AR's precipitation, precipitation where the AR and WCB-ascent overlap, and the MDP change, all considered from the perspective of the AR's maximum IVT occurrence (IVT_{max}). Mean precipitation within the AR area (Figure 8, blue) shows a small increase from -24h until the IVT_{max} and then a pronounced decrease until +24h. The mean precipitation on the AR and WCB-ascent overlap region (Figure 8, red) shows a similar pattern as the AR's mean precipitation but presenting higher values. This shows the ascent's influence on precipitation occurrence within the AR.

For the MDP distribution (considering only the associated ETCs, Figure 9, purple), the values represent the change in SLP for each 6 hours. As we observe in the mean line, the highest decrease in SLP occurs between -6h and +6h of the IVT_{max}. As for the maximum IVT (Figure 9, green), an average of ~1300 $kgm^{-1}s^{-1}$ occurs at peak intensity, with an increase of moisture as the AR develops and a pronounced decrease as precipitation occurs within 6 hours of the AR's peak intensity. Notably, on the AR's peak intensity, the distribution reaches 1800 $kgm^{-1}s^{-1}$. Consistent with Figure 7, the highest precipitation occurs on (and before) the MDP of the ETC, closer to the AR's axis before the intensification of the ETC, where the ascent phase presents a northward extension.

https://doi.org/10.5194/egusphere-2026-2313
Preprint. Discussion started: 27 April 2026
© Author(s) 2026. CC BY 4.0 License.

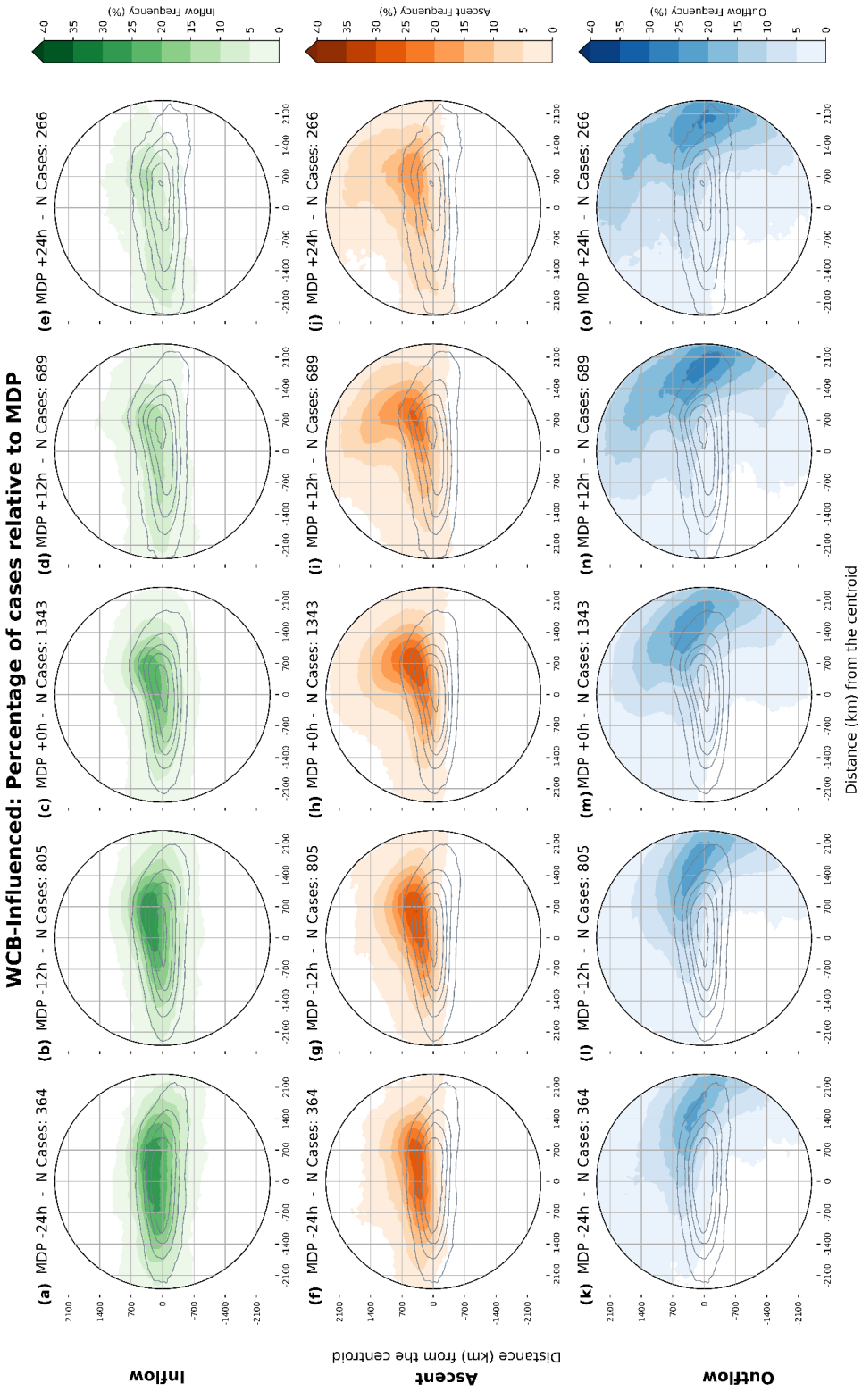

Figure 6: Temporal evolution of WCB phase frequency (%) for WCB-influenced AR events, centered on the time of the associated ETC's MDP. Rows show (a-e) WCB inflow, (f-j) WCB ascent, and (k-o) WCB outflow frequency. Rows show fields at MDP-24h, MDP-12h, MDP, MDP+12h, and MDP+24h. Grey contours represent AR relative frequency (from 10% to 90%).

https://doi.org/10.5194/egusphere-2026-2313
Preprint. Discussion started: 27 April 2026
© Author(s) 2026. CC BY 4.0 License.

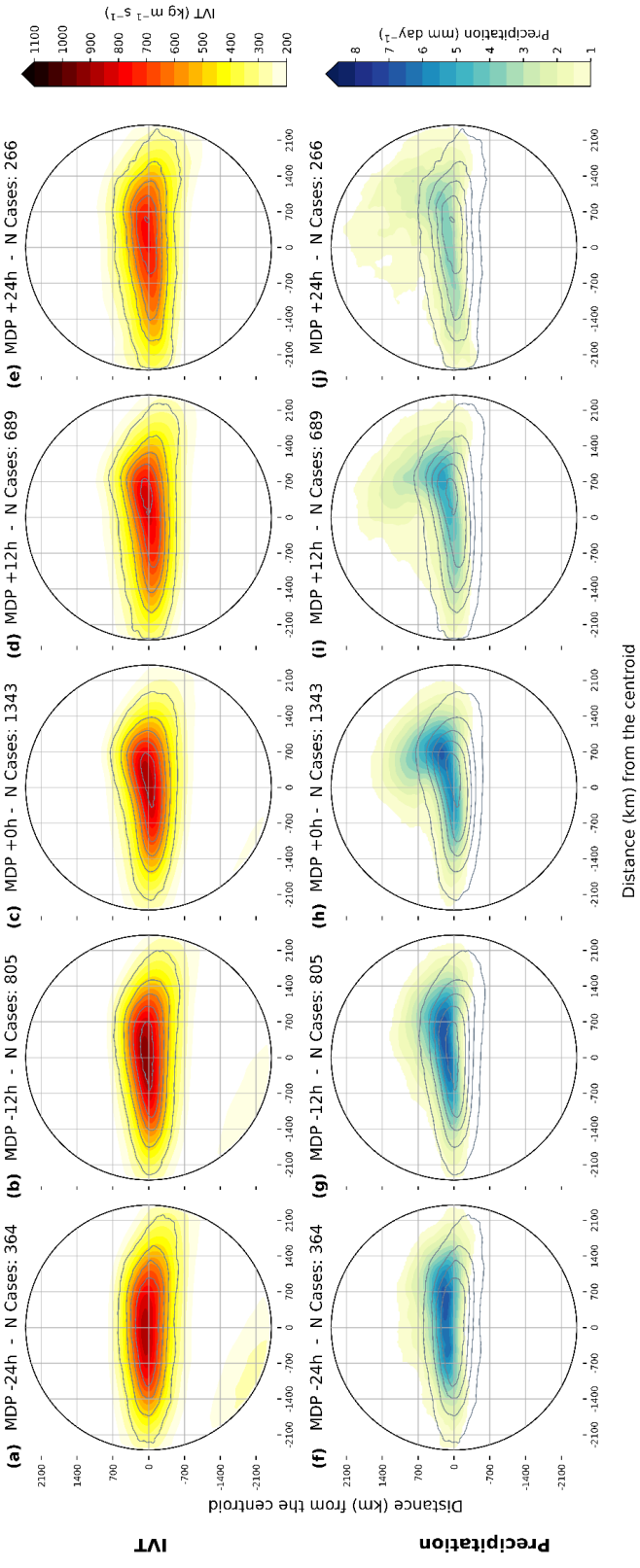

Figure 7: Temporal evolution of composites for WCB-influenced AR events, around the ETC's MDP (same timeline as Fig- 6). Top row (a-e): IVT ($kg\,m^{-1}\,s^{-1}$/AR). Bottom row (f-j): Total precipitation (mm/AR).

https://doi.org/10.5194/egusphere-2026-2313
Preprint. Discussion started: 27 April 2026
© Author(s) 2026. CC BY 4.0 License.

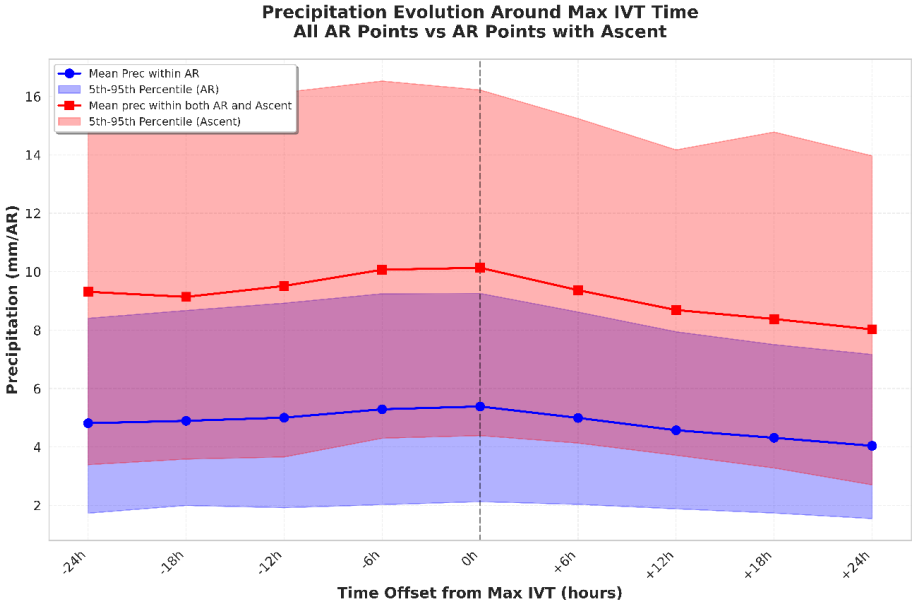

Figure 8: Precipitation change relative to the time of maximum IVT within the AR (0h). The blue line shows the mean precipitation and the blue shading represents the precipitation distribution between the 5th and 95th percentiles over the entire AR area, while the red line shows the mean precipitation and the red shading represents the precipitation distribution between the 5th and 95th percentiles over the region where the AR and the ascent overlap (i.e., the superimposed area).

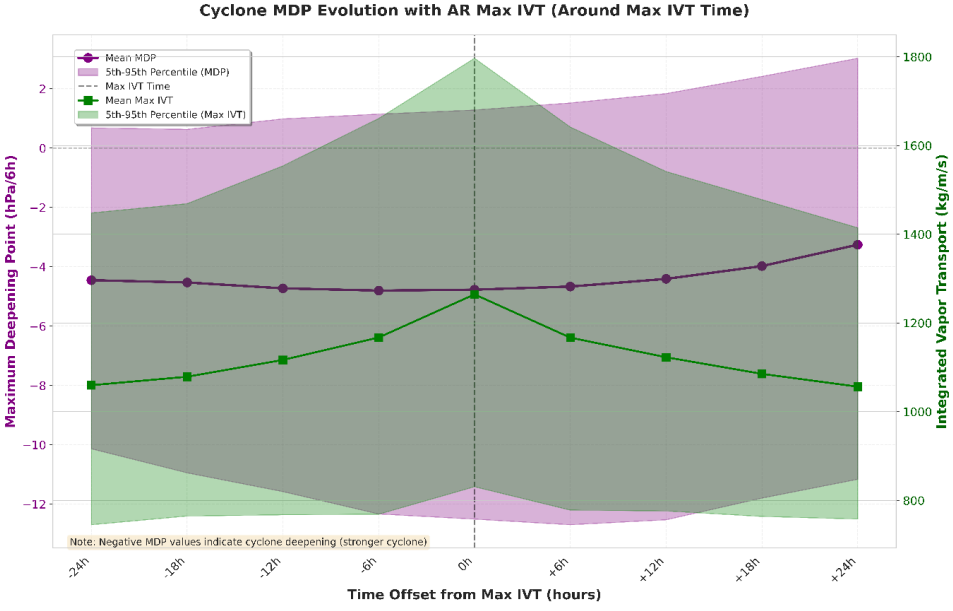

Figure 9: Evolution of IVT (green) and the associated MDP (purple) around the time of maximum IVT within the AR. The maximum IVT is defined as the highest IVT value within the AR area. MDP is calculated for each ETC that has an associated AR. Shading colours represent the distribution of MDP (purple) and Max IVT (green) between the 5th and 95th percentiles.

https://doi.org/10.5194/egusphere-2026-2313
Preprint. Discussion started: 27 April 2026
© Author(s) 2026. CC BY 4.0 License.

6 Conclusions

The aim of this study was to perform a composite-based analysis, to systematically quantify the dynamical linkage between atmospheric rivers (ARs), warm conveyor belts (WCBs), and extratropical cyclones (ETCs) over the North Atlantic. This integrated methodology addresses a critical gap in understanding the spatial misalignment between the core of maximum IVT, which defines the AR, and the region of strongest WCB-ascent which is a driver of precipitation (Pfahl et al., 2014). The main conclusions are formulated below as answers to our research questions as follows:

- *How does the presence or absence of the WCB ascent phase influence the intensity and spatial distribution of precipitation within ARs, i.e., how different are the AR characteristics when the ascent phase is present within the AR?*

  Composite analysis reveals that ARs coupled with WCB ascent exhibit stronger IVT (exceeding 1100 kg m^{-1} s^{-1}) and a broader spatial extent compared to AR-only events. This intensification is supported by enhanced low-level convergence, observed in the WCB inflow region, located predominantly north of the AR core. WCB ascent phase appears to dictate the location and intensity of the precipitation field. While both AR classes transport large moisture amounts, only WCB-coupled events generate heavy precipitation maxima (>8 mm/day) shifted northeast of the AR centroid. In AR-only cases, precipitation is substantially weaker and forms a diffuse northeastward extent towards the cyclone center (with values lower than 5 mm), likely linked to synoptic-scale uplift, the WCB is not strong enough to be detected by the ELIAS model, residual ascent from prior WCB activity or frontal related precipitation.

- *How does the AR-WCB association evolve during the lifecycle of the associated ETC particularly around the time of maximum deepening point (MDP)?*

  Temporal composites around the ETC's MDP illustrate a dynamic sequence: (i) (-24h to -12h) strong WCB inflow, potentially allowing the inflow of moisture into the developing AR. (ii) (MDP) WCB ascent, AR IVT, and precipitation all peak simultaneously, with the precipitation pattern resembling the ascent footprint. (iii) (+12h to +24h) ascent weakens, while WCB outflow peaks, and the number of ARs decreases as moisture is removed through precipitation.

The climatological interplay among ARs, WCBs, and ETCs in the North Atlantic constitutes a tightly coupled, process-driven system (Dacre et al., 2019; Dacre and Clark 2025). Their three-phase structure is physically inseparable from ETC dynamics: the WCB inflow forces the wind convergence in the boundary-layer; the AR is the signature of the organized transport of moisture, usually located equatorward of the low's center; and the WCB ascent forces the moisture upward, leading to precipitation formation and the release of latent heat reinforcing the cyclone's circulation (Sodemann et al., 2020). This trio forms a moisture-dynamics-thermodynamics feedback loop, where each component modulates the others' intensity and lifecycle.

The region where the highest precipitation matches with the highest WCB-ascent occurrence coincides with the typical location of the cyclone's warm front, where large-scale uplift and conditional symmetric instability can trigger deep convection (Wernli and Gray 2024). This indicates that the WCB's organized ascent is the primary mechanism converting AR moisture into intense rainfall, a distinction crucial for operational forecasting, as it demonstrates that extreme precipitation is not merely a result of high moisture content but also strongly associated to the presence and location of strong ascent. The temporal evolution throughout the ETC development, with key transitions occurring within narrow ±12-hour windows, highlights the dynamical link, where the frequency of WCB ascent, the magnitude of IVT, and the spatial extent and intensity of precipitation all reach their maximum values at the exact time of the cyclone's most rapid deepening. This maximum ascent coinciding with the cyclone's strongest intensification is consistent with the climatological WCB lifecycle documented by Heitmann et al.

https://doi.org/10.5194/egusphere-2026-2313
Preprint. Discussion started: 27 April 2026
© Author(s) 2026. CC BY 4.0 License.

(2024) for the North Atlantic, who similarly found that the most rapidly ascending WCBs are associated with the highest precipitation rates.

For forecasting, this means that accurately predicting the timing and location of the MDP is of upmost importance, as it serves as the point for the entire sequence of high-impact weather. This coupling explains the forecast errors documented by Lavers et al. (2020) and Li et al. (2024), where inaccuracies in the jet stream or initial moisture fields propagate through the system, leading to significant errors in the predicted location and intensity of the AR and its associated extreme precipitation. Understanding this integrated lifecycle is therefore essential for improving the skill of numerical weather prediction models in anticipating the most severe midlatitude hydrological extremes. This integrated perspective aligns with the kinematic framework proposed by Dacre and Clark (2025), who demonstrated that despite varying methodologies and terminology, the underlying mechanisms driving ARs, WCBs, and ETCs are fundamentally consistent. Their analysis reinforces that these features are not merely co-located but represent different manifestations of a unified atmospheric flow pattern, supporting our conclusion that forecasting skill requires treating them as a coupled system. In addition, the sensitivity of WCB ascent characteristics to cloud microphysical parameterizations and inflow environmental conditions, as quantified by Oertel et al. (2025), further increase these forecast challenges. Their perturbed parameter ensemble demonstrates that uncertainties in the representation of microphysical processes locally modify vertical velocity along the WCB and determine precipitation efficiency, with distinct impacts on the spatial distribution and intensity of precipitation, precisely the features our composite analysis identifies as critical for extreme event outcomes.

Our new results have significant implications for both weather prediction and climate modelling. Operational models often struggle to accurately represent the timing and location of AR-related precipitation extremes, partly because they may not adequately resolve the mesoscale dynamics that govern the interaction between the AR's moisture plume and the WCB's ascent. The finding that precipitation maxima are displaced from the IVT core underscores the need for forecast verification metrics that assess not just the AR's position and intensity but also the model's ability to correctly simulate the location of frontal ascent and embedded convection. Moreover, ongoing climate change are expected to change both in cyclone (Catto et al., 2019) and AR characteristics (Payne et al., 2020). This reinforces our conclusion that the dynamic component will ultimately determine future flood risk severity, requiring that climate models adequately resolve these process interactions.

Looking forward, this composite analysis should be expanded to other Ocean basins to assess the universality of these dynamics. The critical role of the WCB in converting moisture to extreme precipitation is underscored by previous work. For example, Catto et al. 2015 has demonstrated the role of the WCB to produce extreme precipitation events (EPEs), when matched with fronts. This link was found to be between 2 and 10 times more critical to EPE occurrence than when considering fronts alone. Another study, by Pfahl et al. 2014, has showed that the percentage of extreme precipitation associated with a WCB is higher than 70%-80%. Building on this, our findings suggest that future work must use convection-permitting models to investigate the role of embedded convection within WCBs, a process that these studies identified as a key amplifier that our composite analysis could not fully resolve. Addressing this gap is essential for understanding how the dynamic coupling identified here will shape the most severe midlatitude hydrological extremes in a warming climate.

Acknowledgements

This work was supported by the Portuguese Science Foundation (FCT) I.P./MCTES through the project AMOTHEC (DRI/India/0098/2020) with DOI 10.54499/DRI/India/0098/2020 (https://doi.org/10.54499/DRI/India/0098/2020) and through national funds (PIDDAC): LA/P/0068/2020 – (https://doi.org/10.54499/LA/P/0068/2020), UID/50019/2025 - (https://doi.org/10.54499/UID/50019/2025), UID/PRR/50019/2025 - (https://doi.org/10.54499/UID/PRR/50019/2025), UID/PRR2/50019/2025. TMF was supported by FCT through PhD grant UI/BD/154496/2022. SC and JGP contributions were funded by the German Federal Ministry of Research, Technology and Space (BMFTR), ClimXtreme2 program, subproject "A6 Intensity and structural changes of extreme midlatitude cyclones in a warming climate" (01LP2322A). JGP thanks AXA Research Fund for support. The contribution of JQ was funded by the European Union (ERC, ASPIRE, 101077260). AMR was supported by the Helmholtz "Changing Earth – Sustaining our Future" program.

https://doi.org/10.5194/egusphere-2026-2313
Preprint. Discussion started: 27 April 2026
© Author(s) 2026. CC BY 4.0 License.

Data Availability

ERA5 reanalyses are available from the Copernicus Climate Data Store (https://doi.org/10.24381/CDS.ADBB2D47, Copernicus Climate Change Service, 2023). The WCB data was acessed through the LSDF Online Storage service of KIT (Karlsruhe Institute of Technology), provided by Quinting and Grams (2022). The exact version of the time-lag models, the decision thresholds, the 30d running mean trajectory-based WCB climatology, and code to process the input data for the models are archived on Zenodo (https://doi.org/10.5281/zenodo.5154980, Quinting and Grams, 2021). The ETC data was provided by Svenja Christ.

Author Contributions

AMR, RMT, JGP, JQ and TMF conceived and designed the study. TMF performed the data analysis and prepared the figures. AMR, RMT, JQ, SC and JGP contributed with methodologies and data. The initial draft was written by TMF, supported by RMT, AMR, JQ, SC and JGP. All authors contributed to discussions, comments, and text revisions.

References

Asharaf, S., Guan, B., and Waliser, D. E.: ROTATE: A coordinate system for analyzing atmospheric rivers. Geophysical Research Letters, 51, e2023GL106736. https://doi.org/10.1029/2023GL106736, 2024.

Binder, H., Boettcher, M., Joos, H., and Wernli, H.: The Role of Warm Conveyor Belts for the Intensification of Extratropical Cyclones in Northern Hemisphere Winter. Journal of the Atmospheric Sciences, 73(10), 3997-4020. https://doi.org/10.1175/JAS-D-15-0302.1, 2016.

Carlson, T. N.: Airflow Through Midlatitude Cyclones and the Comma Cloud Pattern. *Monthly Weather Review*, *108*(10), 1498-1509. https://doi.org/10.1175/1520-0493(1980)108<1498:ATMCAT>2.0.CO;2, 1980.

Catto, J. L., Madonna, E., Joos, H., Rudeva, I., and Simmonds, I.: Global Relationship between Fronts and Warm Conveyor Belts and the Impact on Extreme Precipitation. Journal of Climate, 28(21), 8411-8429. https://doi.org/10.1175/JCLI-D-15-0171.1, 2015.

Catto, J. L., Shaffrey, L. C., and Hodges, K. I.: Can Climate Models Capture the Structure of Extratropical Cyclones?. Journal of Climate, 23(7), 1621-1635. https://doi.org/10.1175/2009JCLI3318.1, 2010.

Catto, J.L., Ackerley, D., Booth, J.F., Champion, A.J., Colle, B.A., Pfahl, S., Pinto, J.G., Quinting, J.F., and Seiler, C.: The Future of Midlatitude Cyclones. Current Climate Change Reports 5, 407–420. https://doi.org/10.1007/s40641-019-00149-4, 2019.

Christ, S., Quinting, J. and Pinto, J.G.: Characteristics of diabatically influenced cyclones with high wind damage potential in Europe. Quarterly Journal of the Royal Meteorological Society, e70083. Available from: https://doi.org/10.1002/qj.70083, 2025.

Coll-Hidalgo, P., Gimeno-Sotelo, L., Fernández-Alvarez, J.C., Nieto, R., and Gimeno, L.: North Atlantic Extratropical Cyclone Tracks and Lagrangian-Derived Moisture Uptake Dataset. Sci Data 11, 1258. https://doi.org/10.1038/s41597-024-04091-5, 2024.

Dacre, H. F., Clark, P. A., Martinez-Alvarado, O., Stringer, M. A., and Lavers, D. A.: How do atmospheric rivers form?, B. Am. Meteorol. Soc., 96, 1243–1255, https://doi.org/10.1175/BAMS D-14-00031.1, 2015.

Dacre, H. F., Martínez-Alvarado, O., and Mbengue, C. O.: Linking atmospheric rivers and warm conveyor belt airflows, J. Hydrometeorol., 20, 1183–1196, https://doi.org/10.1175/JHM-D 18-0175.1, 2019.

Dacre, H.F., Clark, P.A.: A kinematic analysis of extratropical cyclones, warm conveyor belts and atmospheric rivers. npj Clim Atmos Sci 8, 97. https://doi.org/10.1038/s41612-025-00942-z, 2025.

Dacre, H.F.: A review of extratropical cyclones: observations and conceptual models over the past 100 years. Weather, 75: 4-7. https://doi.org/10.1002/wea.3653, 2020.

https://doi.org/10.5194/egusphere-2026-2313
Preprint. Discussion started: 27 April 2026
© Author(s) 2026. CC BY 4.0 License.

Eiras-Barca, J., Ramos, A. M., Pinto, J. G., Trigo, R. M., Liberato, M. L. R., and Miguez-Macho, G.: The concurrence of atmospheric rivers and explosive cyclogenesis in the North Atlantic and North Pacific basins, Earth Syst. Dynam., 9, 91–102, https://doi.org/10.5194/esd-9-91-2018, 2018.

Eiras-Barca, J., S. Brands, and G. Miguez-Macho: Seasonal variations in North Atlantic atmospheric river activity and associations with anomalous precipitation over the Iberian Atlantic Margin, J. Geophys. Res. Atmos., 121, 931–948, doi:10.1002/2015JD023379, 2016.

Federer, M., Papritz, L., Sprenger, M., and Grams, C. M.: Synoptic perspective on the conversion and maintenance of local available potential energy in extratropical cyclones, Weather Clim. Dynam., 6, 211–230, https://doi.org/10.5194/wcd-6-211-2025, 2025.

Fernández-Alvarez, J.C., Pérez-Alarcón, A., Eiras-Barca, J. et al. Projected changes in atmospheric moisture transport contributions associated with climate warming in the North Atlantic. Nat Commun 14, 6476. https://doi.org/10.1038/s41467-023-41915-1, 2023.

Ferreira, T. M., Trigo, R. M., Gaspar, T. H., Pinto, J. G., and Ramos, A. M.: The record-breaking precipitation event of December 2022 in Portugal, Nat. Hazards Earth Syst. Sci., 25, 609–623, https://doi.org/10.5194/nhess-25-609-2025, 2025a.

Ferreira, T.M., Gaspar, T.H., Molina, M.O., Trigo, R.M., Deus, R. and Ramos, A.M.: Extreme rainfall in Madeira: the June 2023 weather event. Weather. https://doi.org/10.1002/wea.7786, 2025b.

Fink, A. H., Brücher, T., Ermert, V., Krüger, A., and Pinto, J. G.: The European storm Kyrill in January 2007: synoptic evolution, meteorological impacts and some considerations with respect to climate change, Nat. Hazards Earth Syst. Sci., 9, 405–423, https://doi.org/10.5194/nhess-9-405-2009, 2009.

Gershunov, A., T. Shulgina, F. M. Ralph, D. A. Lavers, and J. J. Rutz: Assessing the climate-scale variability of atmospheric rivers affecting western North America, Geophys. Res. Lett., 44, 7900–7908, doi:10.1002/2017GL074175, 2017.

Gimeno, L., Nieto, R., Vázquez, M., and Lavers, D.A.: Atmospheric Rivers: a mini-review. Frontiers in Earth Science, Volume 2, ISSN=2296-6463, DOI=10.3389/feart.2014.00002, 2014.

Glinton, M. R., Gray, S. L., Chagnon, J. M. and Morcrette, C. J.: Modulation of precipitation by conditional symmetric instability release. Atmospheric Research. 185 186–201, https://doi.org/10.1016/j.atmosres.2016.10.013, 2017.

Guo, Y., Shinoda, T., Guan, B., Waliser, D. E., and Chang, E. K. M.: Statistical relationship between atmospheric rivers and extratropical cyclones and anticyclones. Journal of Climate, 33(18), 7817–7834. https://doi.org/10.1175/JCLI-D-19-0126.1, 2020.

Heitmann, K., Sprenger, M., Binder, H., Wernli, H., and Joos, H.: Warm conveyor belt characteristics and impacts along the life cycle of extratropical cyclones: case studies and climatological analysis based on ERA5, Weather Clim. Dynam., 5, 537–557, https://doi.org/10.5194/wcd-5-537-2024, 2024.

Hersbach, H., Bell, B., Berrisford, P., Hirahara, S., Horányi, A., Muñoz-Sabater, J., Nicolas, J., Peubey, C., Radu, R., Schepers, D., Simmons, A., Soci, C., Abdalla, S., Abellan, X., Balsamo, G., Bechtold, P., Biavati, G., Bidlot, J., Bonavita, M., Chiara, G., Dahlgren, P., Dee, D., Diamantakis, M., Dragani, R., Flemming, J., Forbes, R., Fuentes, M., Geer, A., Haimberger, L., Healy, S., Hogan, R.J., Hólm, E., Janisková, M., Keeley, S., Laloyaux, P., Lopez, P., Lupu, C., Radnoti, G., Rosnay, P., Rozum, I., Vamborg, F., Villaume, S. and Thépaut, J.N.: The ERA5 global reanalysis. Quarterly Journal of the Royal Meteorological Society, 146(730), 1999–2049. https://doi.org/10.1002/qj.3803, 2020.

Hoskins, B. J., and Hodges, K. I.: New Perspectives on the Northern Hemisphere Winter Storm Tracks. Journal of the Atmospheric Sciences, 59(6), 1041-1061. https://doi.org/10.1175/1520-0469(2002)059<1041:NPOTNH>2.0.CO;2, 2002.

Joos, H.: Warm Conveyor Belts and Their Role for Cloud Radiative Forcing in the Extratropical Storm Tracks. Journal of Climate, 32(16), 5325-5343. https://doi.org/10.1175/JCLI-D-18-0802.1, 2019.

Lavers, D. A., Ingleby, N. B., Subramanian, A. C., Richardson, D. S., Ralph, F. M., Doyle, J. D., Reynolds, C. A., Torn, R. D., Rodwell, M. J., Tallapragada, V., and Pappenberger, F.: Forecast Errors and Uncertainties in Atmospheric Rivers. Weather and Forecasting, 35(4), 1447-1458. https://doi.org/10.1175/WAF-D-20-0049.1, 2020.

Lavers, D. A., Villarini, G., Allan, R. P., Wood, E. F., and Wade, A. J.: The detection of atmospheric rivers in atmospheric reanalyses and their links to British winter floods and the large-scale climatic circulation. J. Geophys. Res.-Atmos., 117, D20106, https://doi.org/10.1029/2012JD018027, 2012.

https://doi.org/10.5194/egusphere-2026-2313
Preprint. Discussion started: 27 April 2026
© Author(s) 2026. CC BY 4.0 License.

Li, L., Shao, A., Qiu, X.: Short-term forecast large-scale error characteristics and their relationship with precipitation forecast skill under two rainfall regimes. Atmospheric Research, Volume 298, 107152, ISSN 0169-8095, https://doi.org/10.1016/j.atmosres.2023.107152, 2024.

Lopez-Marti, F., Czaja, A., Messori, G. and Rutgersson, A.: Modulation of North Atlantic atmospheric rivers by the Gulf Stream. Quarterly Journal of the Royal Meteorological Society, e70153. Available from: https://doi.org/10.1002/qj.70153, 2026.

Lopez-Marti, F., Ginesta, M., Faranda, D., Rutgersson, A., Yiou, P., Wu, L., and Messori, G.: Future changes in compound explosive cyclones and atmospheric rivers in the North Atlantic, Earth Syst. Dynam., 16, 169–187, https://doi.org/10.5194/esd-16-169-2025, 2025.

Luís, D., Gama, C., Gonçalves, C., Castanheira, J. M., Ramos, A. M., Sprenger, M., and Gorodetskaya, I. V.: Atmospheric rivers in the Iberian Peninsula: Connection with extratropical fronts and precipitation. Journal of Geophysical Research: Atmospheres, 130, e2025JD043891. https://doi.org/10.1029/2025JD043891, 2025.

Ma, X., Jia, Y. and Han, Z.: Impact of the Gulf Stream front on atmospheric rivers and Rossby wave train in the North Atlantic. Clim Dyn 62, 5827–5843. https://doi.org/10.1007/s00382-024-07178-2, 2024.

Madonna, E., Wernli, H., Joos, H., and Martius, O.: Warm Conveyor Belts in the ERA-Interim Dataset (1979–2010). Part I: Climatology and Potential Vorticity Evolution. Journal of Climate, 27(1), 3-26. https://doi.org/10.1175/JCLI-D-12-00720.1, 2014.

Mahto, S. S., Nayak, M. A., Lettenmaier, D. P., and Mishra, V.: Atmospheric rivers that make landfall in India are associated with flooding, Commun. Earth Environ., 4, 120, https://doi.org/10.1038/s43247-023-00775-9, 2023.

McErlich, C., McDonald, A., Renwick, J., and Schuddeboom, A.: An assessment of extra-tropical cyclone precipitation extremes over the Southern Hemisphere using ERA5. Geophysical Research Letters, 50, e2023GL104130. https://doi.org/10.1029/2023GL104130, 2023.

Murray, R.J. and Simmonds, I.: A numerical scheme for tracking cyclone centres from digital data. Part I: Development and operation of the scheme. Aust. Met. Mag., 39, 155-166. https://www.cawcr.gov.au/projects/cyclone-exchange/Murray_and_Simmonds_1991a_AMM.pdf, 1991.

Neu, U., Akperov, M. G., Bellenbaum, N., Benestad, R., Blender, R., Caballero, R., Cocozza, A., Dacre, H. F., Feng, Y., Fraedrich, K., Grieger, J., Gulev, S., Hanley, J., Hewson, T., Inatsu, M., Keay, K., Kew, S. F., Kindem, I., Leckebusch, G. C., Liberato, M. L. R., Lionello, P., Mokhov, I. I., Pinto, J. G., Raible, C. C., Reale, M., Rudeva, I., Schuster, M., Simmonds, I., Sinclair, M., Sprenger, M., Tilinina, N. D., Trigo, I. F., Ulbrich, S., Ulbrich, U., Wang, X. L., and Wernli, H.: IMILAST: A Community Effort to Intercompare Extratropical Cyclone Detection and Tracking Algorithms: . Bulletin of the American Meteorological Society, 94(4), 529-547. https://doi.org/10.1175/BAMS-D-11-00154.1, 2013.

Oertel, A., Boettcher, M., Joos, H., Sprenger, M., and Wernli, H.: Potential vorticity structure of embedded convection in a warm conveyor belt and its relevance for large-scale dynamics, Weather Clim. Dynam., 1, 127–153, https://doi.org/10.5194/wcd-1-127-2020 , 2020.

Oertel, A., Boettcher, M., Joos, H., Sprenger, M., Konow, H., Hagen, M., and Wernli, H.: Convective activity in an extratropical cyclone and its warm conveyor belt – a case-study combining observations and a convection-permitting model simulation, Q. J. Roy. Meteor. Soc., 145, 1406–1426, https://doi.org/10.1002/qj.3500, 2019.

Oertel, A., Miltenberger, A.K., Grams, C.M. and Hoose, C.: Sensitivities of warm conveyor belt ascent, associated precipitation characteristics and large-scale flow pattern: Insights from a perturbed parameter ensemble. Quarterly Journal of the Royal Meteorological Society, 151(770), e4986, https://doi.org/10.1002/qj.4986, 2025.

Oertel, A., Sprenger, M., Joos, H., Boettcher, M., Konow, H., Hagen, M., and Wernli, H.: Observations and simulation of intense convection embedded in a warm conveyor belt – how ambient vertical wind shear determines the dynamical impact, Weather Clim. Dynam., 2, 89–110, https://doi.org/10.5194/wcd-2-89-2021, 2021.

Payne, A.E., Demory, ME., Leung, L.R., Ramos, A.M., Sheilds, C.A., Rutz, J.J., Siler, N., Villarini, G., Hall, A., and Ralph, F.M.: Responses and impacts of atmospheric rivers to climate change. Nat Rev Earth Environ 1, 143–157. https://doi.org/10.1038/s43017-020-0030-5, 2020.

Peng, Y.-M., Fu, G., Li, P.-Y., and Ni, J.: Characteristics of super atmospheric rivers associated with explosive extratropical cyclones over the Northern Pacific Ocean. Geophysical Research Letters, 52, e2025GL114654. https://doi.org/10.1029/2025GL114654, 2025.

https://doi.org/10.5194/egusphere-2026-2313
Preprint. Discussion started: 27 April 2026
© Author(s) 2026. CC BY 4.0 License.

Pfahl, S., Madonna, E., Boettcher, M., Joos, H., and Wernli, H.: Warm Conveyor Belts in the ERA-Interim Dataset (1979–2010). Part II: Moisture Origin and Relevance for Precipitation. Journal of Climate, 27(1), 27-40. https://doi.org/10.1175/JCLI-D-13-00223.1, 2014.

Pinto, J. G., Spangehl, T., Ulbrich, U. and Speth, P.: Sensitivities of a cyclone detection and tracking algorithm: individual tracks and climatology. Meteorologische Zeitschrift,14,823–838, DOI: 10.1127/0941-2948/2005/0068, 2005.

Pinto, J. G., Zacharias, S., Fink, A. H., Leckebusch, G. C., and Ul brich, U.: Factors contributing to the development of extreme North Atlantic cyclones and their relationship with the NAO, Clim. Dynam., 32, 711–737, https://doi.org/10.1007/s00382-008-0396-4, 2009.

Quinting, J. and Grams, C. M.: EuLerian Identification of ascending AirStreams (ELIAS 2.0) in Numerical Weather Prediction and Climate Models, Zenodo [code], https://doi.org/10.5281/zenodo.5154980, 2021.

Quinting, J. F. and Grams, C. M.: EuLerian Identification of ascending AirStreams (ELIAS 2.0) in numerical weather prediction and climate models – Part 1: Development of deep learning model, Geosci. Model Dev., 15, 715–730, https://doi.org/10.5194/gmd-15-715-2022, 2022.

Ralph, F. M., Dettinger, M. D., Cairns, M. M., Galarneau, T. J., and Eylander, J.: Defining “Atmospheric River”: How the Glossary of Meteorology Helped Resolve a Debate. Bulletin of the American Meteorological Society, 99(4), 837-839. https://doi.org/10.1175/BAMS-D-17-0157.1, 2018.

Ralph, M. F., Rutz, J. J., Cordeira, J. M., Dettinger, M., Anderson, M., Reynolds, D., Schick, L. J., and Smallcomb, C.: A scale to characterize the strength and impacts of atmospheric rivers. Bulletin of the American Meteorological Society, 100(2), 269–289. https://doi.org/10.1175/BAMS-D-18-0023.1, 2019.

Ramos, A. M., Martins, M. J., Tomé, R., and Trigo, R. M.: Extreme Precipitation Events in Summer in the Iberian Peninsula and Its Relationship With Atmospheric Rivers. Frontiers in Earth Science, Volume 6, 110, DOI=10.3389/feart.2018.00110, 2018b.

Ramos, A. M., Trigo, R. M., Tomé, R., and Liberato, M. L. R.: Impacts of Atmospheric Rivers in Extreme Precipitation on the European Macaronesian Islands. Atmosphere, 9(8), 325. https://doi.org/10.3390/atmos9080325 , 2018a.

Saffin, L., Methven, J., Bland, J., Harvey, B. and Sanchez, C.: Circulation conservation in the outflow of warm conveyor belts and consequences for Rossby wave evolution. Q J R Meteorol Soc, 147(740, 3587–3610. Available from: https://doi.org/10.1002/qj.4143, 2021.

Schemm, S. and Sprenger, M.: Frontal-wave cyclogenesis in the North Atlantic –a climatological characterisation. Q.J.R. Meteorol. Soc., 141: 2989-3005. https://doi.org/10.1002/qj.2584, 2015.

Schultz, D. M., Bosart, L. F., Colle, B. A., Davies, H. C., Dearden, C., Keyser, D., Martius, O., Roebber, P. J., Steenburgh, W. J., Volkert, H., and Winters, A. C.: Extratropical Cyclones: A Century of Research on Meteorology’s Centerpiece. Meteorological Monographs, 59, 16.1-16.56. https://doi.org/10.1175/AMSMONOGRAPHS-D-18-0015.1, 2019.

Schwenk, C. and Miltenberger, A.: The role of ascent timescales for warm conveyor belt (WCB) moisture transport into the upper troposphere and lower stratosphere (UTLS), Atmos. Chem. Phys., 24, 14073–14099, https://doi.org/10.5194/acp-24-14073-2024, 2024.

Sodemann, H., Wernli, H., Knippertz, P., Cordeira, J.M., Dominguez, F., Guan, B., Hu, H., Ralph, F.M., and Stohl, A.: Structure, Process, and Mechanism. In: Ralph, F., Dettinger, M., Rutz, J., Waliser, D. (eds) Atmospheric Rivers. Springer, Cham. https://doi.org/10.1007/978-3-030-28906-5_2, 2020.

Sprenger, M. and Wernli, H.: The LAGRANTO Lagrangian analysis tool– version 2.0, Geosci. Model Dev., 8, 2569–2586, https://doi.org/10.5194/gmd-8-2569-2015, 2015.

Sprenger, M., Fragkoulidis, G., Binder, H., Croci-Maspoli, M., Graf, P., Grams, C. M., Knippertz, P., Madonna, E., Schemm, S., Škerlak, B., and Wernli, H.: Global climatologies of Eulerian and Lagrangian flow features based on ERA-Interim, B. Am. Meteorol. Soc., 98, 1739–1748, https://doi.org/10.1175/BAMS-D-15 00299.1, 2017.

Thandlam, V., Rutgersson, A. and Sahlee, E. Spatio-temporal variability of atmospheric rivers and associated atmospheric parameters in the Euro-Atlantic region. Theor Appl Climatol 147, 13–33. https://doi.org/10.1007/s00704-021-03776-w, 2022.

Trigo, R. M., Osborn, T. J., and Corte-Real, J. M.: The North Atlantic Oscillation influence on Europe: climate impacts and associated physical mechanisms. Climate Research, 20(1), 9–17. http://www.jstor.org/stable/24866789, 2002.

https://doi.org/10.5194/egusphere-2026-2313
Preprint. Discussion started: 27 April 2026
© Author(s) 2026. CC BY 4.0 License.

Uccellini, L. W., and Johnson, D. R.: The Coupling of Upper and Lower Tropospheric Jet Streaks and Implications for the Development of Severe Convective Storms. Monthly Weather Review, 107(6), 682-703. https://doi.org/10.1175/1520-0493(1979)107<0682:TCOUAL>2.0.CO;2, 1979.

Ulbrich, U., Leckebusch, G.C. and Pinto, J.G.: Extra-tropical cyclones in the present and future climate: a review. Theor Appl Climatol 96, 117–131. https://doi.org/10.1007/s00704-008-0083-8, 2009.

Vincent, L.: "Morphological grayscale reconstruction in image analysis: applications and efficient algorithms," in IEEE Transactions on Image Processing, vol. 2, no. 2, pp. 176-201, doi: 10.1109/83.217222, 1993.

Vishnupriya, S., Sprenger, M., Joos, H., and Wernli, H.: The interaction of warm conveyor belt outflows with the upper-level waveguide: a four-type climatological classification, EGUsphere [preprint], https://doi.org/10.5194/egusphere-2025-1731, 2025.

Wernli, H. and Davies, H. C.: A Lagrangian-based analysis of extratropical cyclones. I: The method and some applications, Q. J. Roy. Meteor. Soc., 123, 467–489, https://doi.org/10.1256/smsqj.53810, 1997.

Wernli, H. and Gray, S. L.: The importance of diabatic processes for the dynamics of synoptic-scale extratropical weather systems – a review, Weather Clim. Dynam., 5, 1299–1408, https://doi.org/10.5194/wcd-5-1299-2024, 2024.

Wernli, H., Dirren, S., Liniger, M.A. and Zillig, M.: Dynamical aspects of the life cycle of the winter storm 'Lothar' (24–26 December 1999). Q.J.R. Meteorol. Soc., 128: 405-429. https://doi.org/10.1256/003590002321042036, 2002.

Wernli, H.: A Lagrangian-based analysis of extratropical cyclones. II: A detailed case-study. Quarterly Journal of the Royal Meteorological Society, 123: 1677-1706. https://doi.org/10.1002/qj.49712354211, 1997.

Winters AC.: Kinematic processes contributing to the intensification of anomalously strong North Atlantic jets. Quarterly Journal of the Royal Meteorological Society, 147:2506–2532. https://doi.org/10.1002/qj.4037, 2021.

Woollings, T., and M. Blackburn: The North Atlantic Jet Stream under Climate Change and Its Relation to the NAO and EA Patterns. *J. Climate*, **25**, 886–902, https://doi.org/10.1175/JCLI-D-11-00087.1, 2012.

Woollings, T., Hannachi, A. and Hoskins, B.: Variability of the North Atlantic eddy-driven jet stream. Q.J.R. Meteorol. Soc., 136: 856-868. https://doi.org/10.1002/qj.625, 2010.

Xu, G., Ma, X., Chang, P., and Wang, L.: Image-processing-based atmospheric river tracking method version 1 (IPART-1), Geosci. Model Dev., 13, 4639–4662, https://doi.org/10.5194/gmd-13-4639-2020, 2020.

Zavadoff, B. L., and Kirtman, B. P.: Dynamic and Thermodynamic Modulators of European Atmospheric Rivers. *Journal of Climate*, *33*(10), 4167-4185. https://doi.org/10.1175/JCLI-D-19-0601.1, 2020.

Zhang, Z., Ralph, F. M., and Zheng, M.: The Relationship Between Extratropical Cyclone Strength and Atmospheric River Intensity and Position. Geophysical Research Letters, 46(3), 1814–1823. https://doi.org/10.1029/2018GL079071, 2019.